molecular pharmaceutics

Article

A novel milrinone nanoformulation for use in cardiovascular diseases: preparation and in vitro characterization.

Nikita Lomis, Francis Gaudreault, Meenakshi Malhotra, Susan Westfall, Dominique Shum-Tim, and Satya Prakash

Mol. Pharmaceutics, **Just Accepted Manuscript** • DOI: 10.1021/acs.molpharmaceut.7b00360 • Publication Date (Web): 24 Aug 2017

ACS Publications

Molecular Pharmaceutics is published by the American Chemical Society. 1155 Sixteenth Street N.W., Washington, DC 20036

A novel milrinone nanoformulation for use in cardiovascular diseases: preparation and *in vitro* characterization

Nikita Lomis[1,2], Francis Gaudreault[3], Meenakshi Malhotra[4], Susan Westfall[1], Dominique Shum-Tim[5], Satya Prakash[*]

[1] Biomedical Technology and Cell Therapy Research Laboratory, Department of Biomedical Engineering, 3775 University Street, Montreal, QC, H3A 2B4, Canada

[2] Division of Experimental Medicine, 1110 Pins Avenue, Montreal, QC, H3A 1A3, Canada

[3] Human Health Therapeutics, National Research Council Canada, 6100 Royalmount Avenue, Montreal, QC, H4P 2R2, Canada

[4] Department of Radiology, Stanford University School of Medicine, Stanford, CA, 94305, USA

[5] Division of Cardiac Surgery and Surgical Research, Royal Victoria Hospital, 1001 Boulevard Décarie, Montréal, QC, H4A 3J1, Canada

KEYWORDS: Heart, human serum albumin, nanoparticles, milrinone, targeting, drug delivery

ABSTRACT. Cardiovascular diseases are the leading causes of mortality across the globe. Over the years, various drug formulations and delivery methods have been tested, for cardiac repair. Milrinone (MRN) is a widely known cardiac inotrope drug, used for the treatment of congestive heart failure in patients, however, its efficacy is limited. This study is the first to report the design of a novel MRN-nanoformulation using human serum albumin nanoparticles (HSA-NPs). The HSA-NPs exhibit promising drug delivery characteristics such as target specificity, non-immunogenicity, biocompatibility, and enhanced bioavailability. This article describes a MRN-nanoformulation design for in-vitro drug release, cellular uptake, biocompatibility and other features. The MRN-nanoformulation was prepared by the ethanol desolvation technique and key parameters were optimized to obtain a desired particle size of 154.2±5.8 nm, zeta potential of -29.5±2.9 mV and a drug encapsulation efficiency of 41.1±1.7 %. Molecular docking studies have revealed that MRN binds in the hydrophobic cavity of HSA, which has also been indicated by circular dichroism and enzyme-mediated drug release studies in the presence of trypsin, pepsin, proteinase K, protease and cathepsin D. The intracellular uptake of fluorescently tagged MRN-HSA-NPs using HUVEC and H9c2 cells, was evaluated by flow cytometry. The nanoparticle toxicity results indicated that MRN-HSA-NPs show significantly lower cytotoxicity and higher cell viability ($P<0.0001$) as compared to the MRN-Lactate drug, in HUVEC (61.6±3.7% vs 36.2±2.9%) and H9c2 (58.8±5.7% vs 18.8±4.9%) cells. These studies indicate that the novel MRN-nanoformulation offers better drug delivery procedures than currently used methods and has potential in treatment of congestive heart failure and other cardiovascular diseases.

INTRODUCTION

Cardiovascular diseases (CVDs) are the leading causes of mortality across the developed and developing world, primarily due to unhealthy lifestyles and lack of physical activity [1]. More than 50% of the global CVD occurrences are due to congestive heart failure (CHF), in which buildup of plaque in the coronary artery obstructs the flow of blood to the heart, causing irreversible cardiac necrosis [2]. CHF is commonly treated by use of drugs such as ACE inhibitors, inotropes, beta blockers etc., which lower blood pressure and treat cardiac arrhythmias [3].

Milrinone (MRN), a cardiac inotrope and vasodilator, is widely used for the treatment of CHF. It selectively inhibits the action of the phosphodiesterase III enzyme, increasing the intracellular cAMP concentration, and providing high calcium influx to create a positive inotropic effect [4-6]. Milrinone increases myocardial contractility and decreases systemic vascular resistance, left ventricular filling pressure and pulmonary arterial pressure, thus improving overall cardiac function [7]. It offers an advantage over other cardiac inotropes such as dobutamine, nitroprusside and captopril, in significantly reducing right atrial pressure, pulmonary capillary wedge pressures, left-ventricular end-diastolic pressure along with increase in stroke work index [7]. MRN is commercially available as a lactate formulation (MRN-Lactate) and clinically administered either intravenously or orally to adult as well as pediatric patients for heart failure and related cardiac conditions [8-9]. However, its efficacy may be limited due to lack of target specificity and low bioavailability with other side effects such as renal dysfunction, palpitations and arrhythmias [3, 10].

To improve the target specificity of MRN, we have prepared a MRN-nanoformulation using HSA-NPs. The presence of multiple unique binding pockets on the HSA molecule, promotes the use of HSA-NPs for delivery of various hydrophilic and hydrophobic drugs such as paclitaxel, doxorubicin etc. [11-13]. Milrinone has a half-life of approximately 1-2 hours in humans and is

therefore administered as a continuous intravenous infusion or repeated oral dose[7, 14]. It is widely known that binding the drug to HSA-NPs improves its blood circulation time as compared to that of the free drug itself [15]. Therefore, it is hypothesized that MRN-carrying HSA-NPs will demonstrate superior pharmacokinetics than free MRN , in-vivo. Previous studies have shown that MRN carrying PLGA-NPs were utilized for the treatment of myocardial infarction (MI) in rats, however no in-vivo pharmacokinetics study was performed [16]. Also, the particle size of the PLGA-NPs was approximately 7.4 μm, which is larger than the diameter of the smallest capillaries (approximately 5-6 μm) in the body [17]. A large particle size (> 1 μm) lowers nanoparticle suitability for intravenous delivery. Moreover, HSA-NPs of size less than 250 nm and approximately ±30 mV zeta potential have shown greater physical stability and prolonged blood circulation times [18-20]. Further, unique characteristics like biocompatibility, biodegradability, and non-immunogenicity, have led HSA-NPs to emerge as an excellent choice for delivery of MRN to the heart [21].

In this study, we demonstrate the preparation and optimization of the MRN-HSA-NPs. For the first time, molecular docking has predicted binding between MRN and HSA, also indicated by circular dichroism (CD) spectroscopy. Enzyme mediated drug release studies have been performed to validate MRN encapsulation in HSA-NPs. The cellular uptake of MRN-HSA-NPs was evaluated by fluorescence and flow cytometry studies using HUVEC and H9c2 cells, followed by cell viability analysis comparing the MRN-HSA-NPs with the commercial MRN-Lactate. This novel MRN-nanoformulation is anticipated to be an excellent choice for use in cardiovascular diseases.

EXPERIMENTAL SECTION

Materials. Human serum albumin (> 97% lyophilized) was purchased from Sigma Aldrich (Oakville, ON, Canada). Glutaraldehyde (25% aq. solution) was purchased from Alfa Aesar (Cedarlane, Burlington, ON, Canada). Fluorescein isothiocynate human serum albumin (FITC-HSA) was purchased from Sigma Aldrich (Oakville, ON, Canada). Milrinone was purchased from Selleck Chemicals (Burlington, ON, Canada). Bradford reagent was purchased Bio-Rad (St. Laurent, QC, Canada). Trypsin from bovine pancreas, Pepsin from porcine mucosa, Proteinase K, Cathepsin D from bovine liver and Protease were purchased from Sigma Aldrich (Oakville, ON, Canada). Other chemicals were purchased from Fisher Scientific (Nepean, ON, Canada). LysoTracker Deep Red dye (Thermo Fisher, Mississauga, ON, Canada)

Preparation and optimization of MRN-nanoformulation. HSA-NPs bound to MRN were prepared and optimized by following the ethanol desolvation technique [22]. Briefly, an aqueous solution of HSA was prepared by dissolving 10, 20, 30, 40 and 50 mg of HSA, each, in 1 mL of deionized water and stirred for 10 minutes. The range of these concentrations were selected based on the maximum solubility of HSA in deionized water (50 mg/mL). A stock solution of 1mg/mL milrinone was prepared by dissolving milrinone in minimum amount of DMSO and deionized water for 1 mL volume. The 1 mg/mL solution was diluted by mixing with the preparatory HSA solution in HSA/MRN (μM/μM) ratios of 1:1, 1:5, 1:10 and 1:15. The range of concentrations of MRN selected for optimization were based on the maximum solubility of MRN in DMSO (20 mg/mL). Apart from the solubility of MRN alone, there was a limit to the binding of MRN with HSA in solution. Dissolving higher amounts of MRN with the HSA solution led to precipitation of the drug. The pH of the solution was adjusted to 7.0, 7.5, 8.0, 8.5 and 9.0 by addition of 0.1 M NaOH, while stirring at 800 rpm. The pH of the preparative solution was maintained in the basic range in order to have particles with more negative zeta

potential. Ethanol was added per volume of the HSA solution (1.0, 1.5, 2.0, 2.5 and 3.0) in a dropwise manner, until it turned turbid. The minimum amount of ethanol needed to turn the preparative solution turbid, was to be determined. Glutaraldehyde (8% v/v aq. solution) concentrations of 0.235, 0.588 and 1.175 µL/mg HSA, were added, which correspond to saturation of 40%, 100% and 200% of amino bonds present on the HSA molecule [23]. The mixture was reacted for 4, 8, 18 & 24 hours at room temperature to determine the optimal time needed for glutaraldehyde polymerization to form > 200 nm sized particles. For preparation of fluorescently tagged FITC-HSA-NPs, regular HSA was replaced by FITC-HSA.

The nanoparticles were washed by three rounds of ultracentrifugation at 16500 rpm for 15 minutes each at 25°C [22]. After the final round, the supernatant was collected and pellet was re-dispersed in phosphate buffer saline (PBS). The nanoparticle solution was tip-sonicated for 15 minutes and stored at 4°C until further use.

Nanoparticle characterization, yield and encapsulation efficiency. The average particle size of the nanoparticles was measured by Dynamic Light Scattering (DLS) using a Particle Size Analyzer (Brookhavens Instruments Corporation, NY, USA). The samples were diluted in a 1:20 ratio using deionized water and measured at a scattering angle of 90° and at a temperature of 25°C. The Polydispersity Index (PDI) estimated the size distribution of the nanoparticles. The surface charge of the particles was measured by a Zeta Potential Analyzer (Brookhavens Instruments Corporation, NY, USA), which uses electrophoretic laser Doppler anemometry. The nanoparticle size, shape and surface morphology was examined by Scanning Electron Microscopy (SEM) using Hitachi S-4700 FE-SEM. The nanoparticles were diluted with deionized water and a drop of the diluted suspension was deposited on the polished surface of an

aluminum sample holder. The samples were dried under vacuum and the morphology of the nanoparticles was observed at 5 kV and 50k X magnification.

The nanoparticle yield was measured by UV-Visible spectrophotometry. A standard curve of HSA solution dissolved in Bradford reagent was used as a reference and absorbance was measured at 595 nm. For calculation of yield, the following equation was used:

Yield% = (final amount of HSA in suspension/initial amount of HSA added) * 100.

To measure the encapsulation efficiency, nanoparticles were spin concentrated using Amicon centrifugal filters with a molecular weight cut off (MWCO) of 10,000 Da for non-encapsulated MRN to be eluted out into the collection tube. The concentration of non-encapsulated MRN was determined by UV-Visible spectrophotometry. A standard curve of MRN in a mixture containing DDQ/Ethanol was used as a reference [16, 24]. The absorbance values were measured at 356 nm. The MRN bound to the MRN-HSA-NPs was calculated using the following equation:

Encapsulation Efficiency (EE%) = (amount of MRN encapsulated/ initial amount of MRN added) * 100

Computational modelling of the HSA-MRN complex. Molecular Docking was used to predict the nature of binding, if any, between MRN and HSA. The Protein Data Bank (PDB) was searched to identify target structures of HSA unbound and bound to fatty acids [25]. PDB entries 1HK4, 2BXD and 2BXG bound to the small molecules Thyroxin (THY), Warfarin (RWF) and Ibuprofen (IBP) were used as controls in validating the docking procedure. Fatty acids from the protein target structures were removed before docking the small molecules to allow docking in all interior cavities of HSA. The docking calculations were performed through the Wilma engine

version 0.93 and the predicted conformations were re-scored using SIE (Solvated Interaction Energy) scoring function [26-27]. Conformations of the small molecules were generated in-house. AM1BCC charges (small molecules) were calculated by MolCharge. Sybyl was used to cap N- and C-terminal ends and chain breaks of the targets with NME/ACE groups, rebuild missing side-chain atoms and add explicit Hydrogen atoms [28]. Water molecules were assumed to be non-essential and removed. The protonation and tautomerization states of side-chains of the targets were corrected using the minH algorithm followed by a minimization.

Circular Dichroism Measurement. Circular Dichroism (CD) measurements were carried out on a JASCO spectropolarimeter (model J-810) equipped with a thermoelectrically controlled cell holder under a constant flow of nitrogen gas. The measurements were acquired using a 0.05 mm quartz cell. The spectra were recorded as an average of three scans from 180 – 260 nm, acquired with a scan rate of 20 nm/min at 25°C. The averaged spectra were smoothed with a Savitzky-Golay window of five or seven points. The secondary structure was determined using a CDPro with the CDNN and Deconvolution software [29-30]. For CD measurements, an HSA concentration of 0.2 mg/mL (3 μM) was prepared in deionized water. The HSA/MRN concentrations were in the ratio of 0, 1:1, 1:5, 1:10, 1:15 and 1:20, analyzed at pH 7.0, 8.0 and 9.0. DMSO content (solvent to dissolve MRN) never exceeded 1.0 % (v/v).

Enzymatic drug release from HSA-NPs. The enzymatic drug release from MRN-HSA-NPs was carried out using the following enzymes: trypsin, proteinase K, pepsin, protease and cathepsin D [31]. The MRN-HSA-NPs were divided into aliquots of 1 mL each, with a final nanoparticle concentration of 1 mg/mL and diluted with the respective enzyme buffers. The final enzyme concentration, in the nanoparticle suspension, for trypsin was 100 μg/mL, protease 10 μg/mL, proteinase K 10 μg/mL, pepsin 0.2 mg/mL and cathepsin D 10 μg/mL [31]. The mixture

was incubated at 37°C and 120 rpm. After pre-determined time intervals, the amount of MRN released due to nanoparticle degradation was measured photometrically at 356 nm and the percentage of cumulative release of MRN over time, was calculated.

Cellular uptake of nanoparticles by HUVEC cells and dose-dependent study. The HUVEC cells were received as a kind gift from Dr. Maryam Tabrizian (Dept. of Biomedical Engineering, McGill University, Montreal, QC, Canada). HUVECs were grown in Medium 200 (Thermo Fisher, Mississauga, ON, Canada) supplemented with Low supplement growth serum (Thermo Fisher, Mississauga, ON, Canada). The H9c2 cells (rat cardiomyoblasts) were received as a kind gift from Dr. Renzo Cecere, M.D. (Montreal General Hospital, Montreal, QC, Canada). The H9c2 cells were grown in DMEM (Gibco, Thermo Fisher, Mississauga, ON, Canada) supplemented with 10% FBS (Gibco, Thermo Fisher, Mississauga, ON, Canada). Both the cell lines were maintained in a humidified incubator at 37°C and 5% CO_2.

Intracellular uptake of nanoparticles and their cytotoxic effect was determined by culturing HUVECs at an initial density of 5 x 10^3 cells/well and H9c2 cells at 10 x 10^3 cells/well in black clear bottom 96-well plates. The cells were replaced with fresh media after 24 hours of incubation and treated with MRN-FITC-HSA-NPs and MRN-Lactate. The concentration of MRN in the MRN-FITC-HSA-NPs and MRN-Lactate, was 1000μM, 100μM, 10μM, 1μM, 0.1μM and 0.01μM, diluted with serum-free medium. After 4, 24 and 48 hours of incubation, the cells were washed with PBS and fresh cell culture medium was added. The fluorescence intensity was measured at 489nm/535nm using a Victor3V 1420 Multilabel Counter spectrophotometer (Perkin Elmer, Woodbridge, ON, Canada). After fluorescence measurement, 20 μL of MTT reagent was added to each well containing 100 μL of fresh cell culture medium and incubated in a humidified chamber at 37°C with 5% CO_2. After 4 hours, the cells were lysed

using 100 μL of DMSO and incubated at room temperature for 15 minutes. The absorbance was measured at 570 nm using the Victor3V 1420 Multilabel Counter spectrophotometer

Flow cytometry. Flow cytometry analysis was performed on HUVEC and H9c2 cells. The cells were seeded in 6-well plates at an initial density of $5x10^5$ cells/well with their respective growth media for 48 hours in a humidified incubator at 37°C and 5% CO_2. Post incubation, both the HUVEC and H9c2 cells were exposed to the following treatments: 1) FITC-HSA-NPs (0.2 mg/mL in serum free media), 2) 50 nM of LysoTracker Deep Red dye and 3) FITC-HSA-NPs and LysoTracker Deep Red dye double staining and 4) Untreated [32]. The cells were incubated with the treatments for 1 hour followed by twice washing with PBS. The cells were trypsinized and centrifuged at 1000 rpm for 5 minutes. Flow cytometry was performed on a FACSCanto II (BD Biosciences, San Jose, CA, USA) and data analysis was performed using FlowJo Version 10 (Tree Star Inc., OR, USA) software.

RESULTS

Designing the MRN-nanoformulation. HSA is a α-helical protein, most abundantly found in human plasma, with a molecular weight of 66kDa [21, 33]. It consists of three homologous domains, which are further divided into A and B subdomains. The subdomains IIA and IIIA allow binding of various acidic drugs such as warfarin, diazepam, paclitaxel etc. at either Site 1 or 2, respectively [33]. MRN is a positive inotrope with a bipyridine structure, represented as 2-methyl-6-oxo-1,6-dihydro-3,4'-bipyridine-5-carbonitrile [34]. Studies indicate that the potency of MRN results from the interaction of the methyl moiety with the hydrogen atoms [34-35]. The MRN structure with its electronegative features was anticipated to bind at the Site 1 of the HSA molecule for formation of MRN-HSA-NPs.

Preparation and optimization of the MRN-nanoformulation. In this study, MRN-HSA-NPs were prepared by the ethanol desolvation method [22]. Key parameters were optimized to obtain nanoparticles of size less than 250 nm and zeta potential varying between -15 mV to -40 mV. The parameters considered for optimization were: HSA concentration, MRN concentration, pH of preparative solution, amount of ethanol per volume of HSA solution, glutaraldehyde concentration and glutaraldehyde polymerization time.

Effect of HSA concentration on nanoformulation. The effect of HSA concentration on nanoparticle size and surface charge was determined by preparing nanoparticles at pH 7.0, ethanol/HSA (v/v) ratio 2.0, glutaraldehyde concentration 1.175 µL/mg of HSA and polymerization time of 24 hours. HSA is a negatively charged protein. Thus, increasing the amount of HSA in solution from 10 mg/mL to 50 mg/mL, the particle size increased from 213.2±3.6 nm to 281.8±4.8 nm, due to enhanced formation of intermolecular disulfide bonds **(Figure 1(a))**. Further, the zeta potential decreased from -22.8±1.8 mV to -29.5±2.4 mV **(Figure 1(b))** [13, 36]. The polydispersity index (PDI) for all the preparations was less than 0.15, indicating the homogeneity of the suspension. From this study, the 20 mg/mL HSA concentration, resulting in particle size of 241.8±3.7 nm and zeta potential of -25.5±2.4 mV, was selected for further optimization.

Effect of pH preparative solution on nanoformulation. The pH of the preparative solution was found to influence the size and zeta potential of the nanoparticles. The starting HSA concentration was 20 mg/mL, ethanol/HSA (v/v) ratio was 2.0, glutaraldehyde concentration 1.175 µL/mg HSA and polymerization time of 24 hours. The pH of preparative solution was raised by addition of 0.1 M NaOH, which increases in the negative charges (OH^- ions) in solution. Thus, due to greater repulsion between charges, when pH of the preparative solution

varied from 7.0 to 9.0, particle size decreased from 219.8±0.4 nm to 147.4±1.1 nm **(Figure 1(c))**. As particle aggregation was lowered, the zeta potential of the particles reduced from -23.8±0.8 mV to -26.5±0.2 mV **(Figure 1(d))** [22]. There was no significant difference in the PDI of the particles and was less than 0.15, which indicated homogeneity of the suspension. At pH 8.0, the particle size was 169.1±0.6 nm and zeta potential was -24.1±0.4 mV, and hence, was selected for further optimizations.

Effect of ethanol volume on nanoformulation. The ratio of ethanol/HSA (v/v) was also optimized. The nanoparticles were prepared with a starting HSA concentration of 20 mg/mL, pH 8.0, glutaraldehyde concentration of 1.175 µL/mg HSA and 24 hours polymerization time. Results showed that increasing the ethanol/HSA (v/v) ratio from 1.0 to 3.0 resulted in higher precipitation of the nanoparticles, thus increasing particle aggregation and size from 200.5±2.2 nm to 293.9±5.1 nm, respectively **(Figure 1(e))**. However, since HSA concentration and pH of solution remained constant throughout this optimization, there were no significant differences in the zeta potentials **(Figure 1(f))**. The PDI for all samples was less than 0.15. The ethanol/HSA (v/v) ratio of 1.0 was selected as optimal resulting in particle size of 200.5±2.2 nm and a zeta potential of -27.1±1.8 mV.

Effect of glutaraldehyde on nanoformulation. Glutaraldehyde (8% v/v aqueous solution) concentrations of 0.235, 0.588 and 1.175 µL/mg of HSA, saturating 40%, 100% and 200%, respectively, of the amines present on the HSA molecule, were chosen for optimization [23]. The nanoparticles were prepared at a starting HSA concentration of 20 mg/mL, pH 8.0, ethanol/HSA (v/v) ratio of 1.0 and polymerization time of 24 hours. It was observed that at glutaraldehyde concentration of 0.235 and 0.588 µL/mg of HSA, the particle size was significantly different from that obtained at 1.175 µL/mg of HSA (155.0±0.8, 152.2±2.4 to 175.7±1.6 nm, respectively)

(Figure 1(g)). However, there was no significant difference between the zeta potentials of different samples **(Figure 1(h))**. The PDI for all samples was less than 0.15. The glutaraldehyde concentration 0.588 µL/mg of HSA was considered as optimal.

Effect of MRN concentration on nanoformulation. MRN was added to the HSA solution in the HSA/MRN (µM/µM) ratio of 1:1, 1:5, 1:10 and 1:15. The starting HSA concentration was 20 mg/mL, pH 8.0, ethanol/HSA (v/v) ratio of 2.0, glutaraldehyde 0.588 µL/mg of HSA and polymerization time of 24 hours. It was observed that on increasing the amount of MRN in the HSA solution, the particle size reduced from 384.1±2.9 nm at HSA/MRN (µM/µM) ratios of 1:1 to 224.4±6.3 nm at HSA/MRN (µM/µM) ratios of 1:15, however, there was no significant difference among particle sizes at 1:5, 1:10 and 1:15 **(Figure 1(i))**. This could be due to the electronegative features of the bipyridine rings in the MRN structure. With increasing MRN concentration in the preparative solution, the repulsion between molecules would prevent particle aggregation, thus forming smaller sized particle. Significant differences in the zeta potential of different samples were not observed **(Figure 1(j))**. The PDI of the nanoparticle suspensions was less than 0.15 for all samples. The MRN concentration at HSA/MRN (µM/µM) ratio of 1:15 was selected as optimal.

Effect of glutaraldehyde polymerization time on nanoformulation. The last parameter optimized was the glutaraldehyde polymerization time. The nanoparticles were prepared at 20 mg/mL HSA concentration, HSA/MRN (µM/µM) ratio of 1:15, pH 8.0, ethanol/HSA (v/v) ratio of 2.0 and glutaraldehyde concentration of 0.588 µL/mg of HSA. The MRN-HSA-NPs were reacted for 4, 8, 18 and 24 hours. Results showed that after 24 hours of polymerization, the particle size was 269.5±3.9 nm, which was lower than the particle sizes obtained at other reaction times **(Figure 1(k))**. Glutaraldehyde forms a mesh-like network by undergoing a

condensation reaction with the amine groups present on lysine or hydroxylysine residues present on the albumin [37]. Thus, higher polymerization time possibly allows complete formation of intermolecular bonds and stable nanoparticles. The zeta potential of nanoparticles reacted for 24 hours was -29.0±0.6 mV, which was significantly higher than that of the other samples **(Figure 1(l))**. The PDI for the HSA-NPs reacted for 24 hours was less than that of the other preparations. Thus, the polymerization time of 24 hours was selected as optimized.

SEM analysis of MRN-nanoformulation. MRN-HSA-NPs were prepared by following the ethanol desolvation method and compared with HSA-NPs without MRN, for SEM characterization [22-23]. The size of the MRN-HSA-NPs was 154.2±5.8 nm with a polydispersity index of approximately 0.08 and zeta potential of -29.5±2.9 mV **(Figure 2(a))**. The size of the HSA-NPs was 148.5±6.2 nm with a polydispersity index of approximately 0.19 and zeta potential of -27.1±3.3 mV **(Figure 2(b))**. The yield of the MRN-HSA-NPs was 86.2±2.6% and that of the HSA-NPs was 85.3±2.5%. The milrinone encapsulation efficiency at 1:15 HSA/MRN ratio was 41.7±1.7%, as mentioned in **Table 1**. The particle size for FITC-HSA-MRN-NPs was 130.2±2.0 nm, polydispersity approximately 0.11 and zeta potential was -27.0±0.3 mV. For FITC-HSA-NPs, the particle size was 118.8±1.4 nm, polydispersity index approximately 0.14 and zeta potential was -30.6±1.9 mV.

Molecular Docking study of HSA-MRN interaction. To evaluate the nature of binding between the MRN and HSA, docking simulations were performed with the Wilma software across the entire surface and interior cavities of HSA [27]. The literature data was reproduced by docking the control ligand molecules THY, IBP and RWF **(Figure 3 (a-c))**. All molecules were docked as shown in **Table 2**, i.e. the most energetically favorable conformation as per the Wilma scoring function, a function that quantifies the protein-ligand interactions to estimate binding

affinity. To precisely estimate binding affinities, the analysis was combined with a more elaborate scoring function called SIE scoring function [26].

Docking performed by the SIE-software predicted that MRN was bound to HSA in the sub-pocket that also binds RWF. The MRN molecule was found to exhibit 3-H bond acceptors and a single H-bond donor. The sub-pocket contained the following residues with their side-chains interacting with MRN: GLU292, ALA291, ILE290, SER287, ILE264, ALA261, ILE260, ARG257, HIS242, VAL242, LEU238, LEU234, PHE223, ARG222, LEU219, ARG218, ALA215, TRP214, PHE211, LYS199, GLN196, LYS195, SER192, GLU153 and TYR150. The predictions can be grouped into 2 distinct flipped binding modes: where the nitrogen of the nitrile of MRN interacts with LYS195 **(Figure 3(d))** and where the oxygen of the hydroxyl is highly stabilized via 3 H-bonds formed with ARG257 and TYR150 **(Figure 3(e))**. Predictions also suggest that MRN binds to HSA with a binding affinity similar as that between RWF and HSA. Using the Wilma scoring function, MRN is predicted to bind the strongest to a form of HSA which is bound to fatty acids, in a sub-pocket close to that for RWF **(Figure 3(f))**. However, SIE re-scoring indicates that the MRN binds stronger to a form of HSA which is unbound to fatty acids at the same location **(Figure 3(g))**.

Effect of MRN binding on different HSA conformations. Circular Dichroism is one of the most promising tools for studying various aspects of protein structure [38]. The conformational changes in the secondary structure of HSA have been studied with Far-UV CD, in the range of 180-260 nm at pH 7.0, 8.0 and 9.0. The CD spectra of HSA at pH 7.0, 8.0 and 9.0 exhibits two negative bands in the UV region at 208 nm ($\pi \rightarrow \pi^*$) transition and 222 nm ($n \rightarrow \pi^*$) transition, which is characteristic of an α-helical protein [39]. The conformational states of HSA at pH 7.0, 8.0 and 9.0 contained α-helical content of 58.7%, 62.2% and 59.8%, respectively, which is in

alignment with values reported in the literature [40]. The effect of MRN binding on HSA was studied using Far-UV CD spectra, recorded with MRN/HSA molar ratios of 0, 1:1, 1:5, 1:10, 1:15 and 1:20. At pH 7.0 **(Figure 4(a-b))** and pH 9.0 **(Figure 4(c-d))**, no change in the HSA secondary structure was observed on binding with different MRN concentrations. However, at pH 8.0, a significant reduction in the α-helical content from 62% to 36% at the expense of random coil with 30.7%, was observed at MRN/HSA ratio 1:5. The α-helical content in the remaining preparations with HSA/MRN ratios 1:1, 1:10, 1:15 and 1:20 remained 62.2%, 60.9%, 60.1% and 57.8% respectively **(Figure 4(e-f))**. Similar reduction in helical content of human serum albumin on binding with other drugs has also been reported [41-43]. These results demonstrated the interaction between MRN on binding with HSA at pH 8.0 and have been summarized in **Table 3**.

Enzymatic degradation of HSA-NPs and MRN release. The intracellular delivery of nanoparticles is of utmost importance. In this study, the enzyme mediated release of MRN from MRN-HSA-NPs has been evaluated in the presence of different enzymes such as trypsin, protease and proteinase K which are functionally active at the neutral pH and pepsin, cathepsin D, which are functionally active at acidic pH [31]. The enzyme concentrations in the nanoparticle suspension were set to obtain a rapid nanoparticle degradation and release of MRN. It was observed that trypsin caused rapid degradation of the nanoparticles, releasing 72.5±1.9% of MRN within 24 hours **(Figure 5(a))** whereas pepsin released 87.5±0.9% of MRN within just 2 hours of incubation **(Figure 5(b))**. Proteinase K, protease and cathepsin D exhibited a relatively slower release of 33.4±2.5%, 14.2±2.7% and 5.9±1.3%, respectively, over 24 hours **(Figure 5(c-e))**. A summary of these results is presented in **Table 4**.

Intracellular nanoparticles uptake. It is known that HSA is transported across the endothelial cells by receptor mediated endocytosis via the albondin glycoprotein receptor (gp60) on the surface of endothelial cells [44]. Albumin transports fatty acids across cardiac cells, however, the exact method of HSA uptake by these cells is uncertain [45]. In this study, the uptake of HSA-NPs by HUVECs and H9c2 cells was studied by using FITC-HSA. The HUVECs and H9c2 cells were treated with different concentrations of HSA-NPs with and without MRN, for 4, 24 and 48 hours. The HUVECs treated with MRN-HSA-NPs with nanoparticle concentration of 8000 μg/mL (M-8000) exhibited significantly higher ($P<0.0001$) fluorescence intensity as compared to the other treatments after 4 hours **(Figure 6(a))**. An increase in the fluorescence intensity at nanoparticles concentrations of 600 μg/mL, represented by M-600 (MRN-HSA-NPs) and H-600 (HSA-NPs alone) was observed between 4 hours and 24 hours **(Figure 6(b))**, after which there was no significant increase until 48 hours **(Figure 6(c))**.

The H9c2 rat cardiomyoblasts treated with M-600 and H-600 exhibited higher nanoparticle uptake than M-8000 after 4 hours of treatment **(Figure 7(a))**. The fluorescence intensity further increased significantly ($P<0.0001$) in the M-8000, M-600 and H-600 treatments as compared to rest of the treatments from 4 to 24 hours **(Figure 7(b))** after which there was no significant increase until 48 hours **(Figure 7(c))**. However, no significant cellular uptake of nanoparticles was observed in other treatment conditions.

Flow cytometry analysis. Flow cytometry analysis was performed to validate the uptake of FITC-HSA-NPs (0.2 mg/mL) by HUVECs and H9c2 cells. The treatments were divided as: FITC-HSA-NPs, LysoTracker Deep Red labeled (control), FITC-HSA-NPs and Lysotracker double stained and untreated cells. Results suggested that the for the HUVECs treated with both FITC-HSA-NPs and LysoTracker Deep Red, approximately 98% of the cell population exhibited

fluorescence for both the FITC as well as LysoTracker Deep Red dye **(Figure 8(a))**. For H9c2 cells treated with both FITC-HSA-NPs and LysoTracker Deep Red, approximately 41.3% of the cell population exhibited fluorescence for both FITC and LysoTracker Deep Red dye **(Figure 8(b))**. These results validated the intracellular uptake of the FITC-HSA-NPs.

Cell viability analysis. For evaluating the safety and efficacy of MRN-HSA-NPs on HUVECs and H9c2 cells, the MTT assay was performed. The cells were treated with MRN-HSA-NPs and MRN-Lactate at MRN concentrations 0.01 μM, 0.1 μM, 1 μM, 10 μM, 100 μM and 1000 μM for 4, 24 and 48 hours. Results suggested that the HUVECs incubated with the two treatments containing 1000 μM MRN displayed cell viabilities of 82.4±14.3%, 60.1±3.8%, and 61.6±3.7% at 4, 24 and 48 hours, respectively, in the presence of MRN-HSA-NPs. In comparison, cell viabilities in the presence of MRN-Lactate were 42.5±5.8%, 35.4±0.9% and 36.2±2.9%, respectively **(Figure 9)**. When MRN concentration was 100 μM, the cell viability in the presence of MRN-HSA-NPs was 85.9±12.3%, 71.9±9.6% and 65.1±1.5% at 4, 24 and 48 hours, respectively, whereas for MRN-Lactate treatment was 59.4±4.1%, 49.6±1.1% and 55.7±2.8%, respectively. There were no significant differences in the other MRN-HSA-NPs and MRN-Lactate treatments containing 0.01, 0.1, 1 and 10 μM MRN.

Similarly, the safety of MRN-HSA-NPs as compared to the MRN-Lactate was also evaluated in H9c2 cells. Results suggested that at 1000 μM MRN concentration, the cell viability due to MRN-HSA-NPs was 74.7±3.9%, 74.9±2.2%, and 58.8±5.7% at 4, 24 and 48 hours, respectively, in comparison to that of MRN-Lactate with 52.6±4.9%, 46.1±2.5% and 18.8±4.9%, respectively **(Figure 10)**. At 100 μM MRN concentration, cell viability in the presence of MRN-HSA-NPs was 79.0±0.9%, 88.3±4.1% and 64.9±5.6% at 4, 24 and 48 hours, respectively, whereas in the presence of MRN-Lactate was 62.3±2.1%, 50.1±3.8% and 42.3±10.4%, respectively. Also, there

were no significant differences in the remaining MRN-HSA-NPs and MRN-Lactate treatments containing 0.01, 0.1, 1 and 10 μM MRN. Therefore, it was concluded that the MRN-HSA-NPs exhibited greater cell biocompatibility than MRN-Lactate.

DISCUSSION

HSA-NPs are widely used for the delivery of drugs, genes, hormones, and various other molecules [21]. This study is the first to report the use of HSA-NPs as vehicles for carrying the cardiac inotrope and vasodilator drug, milrinone. MRN is a phosphodiesterase-III inhibitor, which through the action of protein kinase A, improves myocardial contractility. It is commonly administered as a lactate formulation to patients suffering from CHF [5, 34].

This study demonstrates the development of a novel MRN-nanoformulation. Following the ethanol desolvation technique, stable MRN-HSA-NPs were prepared by optimizing key parameters such as HSA and MRN concentration, pH of preparative solution, ethanol volume, glutaraldehyde content and polymerization time [23]. This resulted in achieving an encapsulation efficiency of approximately 41%, which is the highest reported so far. Nanoparticle characterization was performed by the DLS, laser Doppler anemometry and SEM techniques. Molecular docking analysis using the Wilma software predicted a strong binding affinity of -27.6 kcal/mol between MRN and HSA bound to fatty acids, similar to that between warfarin and HSA (-26.6 kcal/mol) [46]. The SIE-rescoring predicted a HSA-MRN binding affinity of -8.6 kcal/mol, when HSA is unbound to fatty acids. MRN is predicted to bind with the Lys195, Arg257 and Tyr150 residues in sub-domain IIA at Site 1 of the HSA molecule, which is also known to bind other hydrophobic drugs [13, 33]. Circular dichroism spectroscopy determined a change in the secondary structure of HSA on interaction with MRN in a 1:5 molar ratio. However, this change

in secondary structure was not observed at other HSA/MRN molar ratios and at other different pH conditions. This can be compared with changes observed in the HSA secondary structure on binding with drug molecules such as virstatin or cisplatin [42-43]. This could be explained due to the changes in molecular conformation of albumin on binding with small molecules, which also change with the pH of solution leading to increased formation of β-sheets and random coil structures at the expense of the α-helix. [47-48]. This may also suggest formation of more inter and intra-domain structures when MRN interacts or binds with HSA. This test was a supplement to our molecular docking studies to indicate that there was an interaction between the MRN and HSA, given that this has not been reported in literature earlier.

An enzyme-mediated drug release study was performed to confirm that MRN was bound to HSA-NPs. The enzymes trypsin, pepsin, proteinase K, protease and cathepsin D were used to evaluate the cumulative MRN release from MRN-HSA-NPs [31]. However, these enzymes may not be physiologically involved when nanoparticles are administered in the body as the drug is expected to be released into the cytosol by receptor mediated endocytosis of the nanoparticles. The rate of degradation of nanoparticles varies due to the difference in the type of peptide bonds cleaved by the enzymes. Trypsin, known to cleave at the carboxyl end of lysine and arginine residues of the protein, released approximately 70-75% of the drug. Pepsin, which cleaves the peptide bonds between phenylalanine, tyrosine and tryptophan residues, released approximately 85-90% of the MRN. However, the drug release in the presence of other enzymes was relatively slower. Cathepsin D, a lysosomal enzyme known for HSA degradation, was unable to completely release MRN from the nanoparticles, possibly due to the high glutaraldehyde concentration [31]. Also, the *in vitro* conditions cannot completely simulate the conditions of a lysosomal vesicle inside the cell.

During in-vivo treatment, MRN-HSA-NPs are anticipated to be up-taken by endothelial cells as well as cardiomyocytes. Therefore, the intracellular uptake and cell biocompatibility of MRN-HSA-NPs was studied using HUVECs and H9c2 cells. Fluorescence studies have revealed that the nanoparticle uptake by both HUVECs and H9c2 cells was time-dependent. This was demonstrated by an increase in fluorescence intensity from 4 to 24 hours at nanoparticle concentrations of 600 and 8000 μg/mL, post which there was no significant increase until 48 hours. Fluorescence intensity at lower nanoparticle concentrations was significantly lower due to high dilution. Further, the presence of MRN in the NPs did not affect their cellular uptake. A flow cytometry analysis confirmed the intracellular uptake of the nanoparticles by both cell types. HUVECs (endothelial cells) are known to interact with HSA through the presence of albondin (gp60) receptors present on the cell surface, which allows receptor mediated endocytosis of the nanoparticles [44]. Also, H9c2 cells (cardiomyoblasts) are anticipated to interact with HSA through the gp18 and gp31 receptors present on the cell surface [45].

Cell viability due to MRN-HSA-NPs and MRN-Lactate was analyzed by performing the MTT assay. The MTT assay is a commonly-used colorimetric assay using the dye 3-(4,5-dimtheylthiazol-2-yl)-2,5-diphenltetrazoliumbromide (MTT) for the rapid determination of cell viability/cytotoxicity [12]. The overall cytotoxicity of the MRN-Lactate treatments was significantly higher than the MRN-HSA-NPs in both HUVEC and H9c2 cells. The treatments which showed very low cytotoxicity, could be attributed to the higher dilution and hence lower nanoparticle uptake as revealed by the fluorescence studies. Therefore, it may be concluded that the MRN-nanoformulation is safer and more biocompatible as compared to the MRN-Lactate.

CONCLUSIONS

The growing incidence of CVDs across the world has also increased the need for developing effective novel technologies. This study is the first to report the development of a novel MRN-nanoformulation using HSA-NPs as vehicles for delivery of milrinone, a cardiac inotrope drug that treats congestive heart failure. MRN-HSA-NPs exhibit a final particle size less than 200 nm and zeta potential of approximately -30 mV, which is ideal for in-vivo drug delivery. This study is also the first to report predictions for MRN binding to the hydrophobic pocket present on sub-domain IIA (Site I) of the HSA molecule, by molecular docking studies.

Future studies will include the determination of the therapeutic effect of the MRN-nanoformulation. Currently, milrinone with a retention time of 1-2 hours, is administered clinically as a continuous intravenous infusion [7, 14]. Hence, pharmacokinetic-pharmacodynamic studies with the MRN-nanoformulation will be useful in determining an increase in the body circulation time of MRN. Since the MRN-nanoformulation is target-specific, it is anticipated to have reduced dose requirements as compared to that of the currently used MRN-Lactate. The intracellular uptake of MRN-HSA-NPs by endothelial cells and cardiomyoblasts as well as their high biocompatibility are indicative that this novel nanoformulation will work better and may potentially be used in CHF and other cardiac applications. Since the presented study is the first of its kind, these results need extrapolation into in-vivo data. Therefore, further animal studies will be required to evaluate the complete clinical potential of the MRN-nanoformulation.

AUTHOR INFORMATION

Corresponding Author

* Email: satya.prakash@mcgill.ca; Tel.: +1-514-398-3676; Fax: +1-514-398-7461

Biomedical Technology and Cell Therapy Research Laboratory, Department of Biomedical Engineering, 3775 University Street, Montreal, QC, H3A 2B4, Canada

Author Contributions

NL conceived, designed and performed the experiments, analyzed the data and wrote the manuscript. FG conducted the molecular docking, analyzed the data and wrote the section on it. MM contributed to conception of idea, data analysis, trouble-shooting and proof-reading of the article. SW contributed to experimental design and proof-reading of the article. DST and SP contributed with the intellectual input and research funding for the study. All authors have given approval to the final version of the manuscript.

ACKNOWLEDGMENTS

This work is supported by the research funding granted to Dr. Satya Prakash from Canadian Institute of Health Research (CIHR) and the Natural Sciences and Engineering Research Council (NSERC). The authors would like to acknowledge the Canadian Graduate Scholarship from NSERC to Ms. Susan Westfall. The authors are grateful to Dr. Enrico Purisima (National Research Council Canada) for supervising the molecular docking study and Hervé Hogues (National Research Council Canada) for performing docking and re-scoring calculations. The authors would like to thank Mr. Xue Dong Liu for assistance in F-50 SEM imaging (Facility for Electron Microscopy Research, Materials Engineering, McGill University).

ABBREVIATIONS

CVDs cardiovascular diseases; CHF congestive heart failure; ACE Angiotensin Converting Enzyme; CABG coronary artery bypass grafting; MRN Milrinone; cAMP cyclic adenosine monophosphate; SR sarcoplasmic reticulum; IGF-1 insulin-like growth factor -1; DDQ 2,3-

Dichloro-5,6-dicyano-p-benzoquinone; DLS Dynamic Light Scattering; SEM Scanning Electron Microscopy; THY Thyroxine; IBF Ibuprofen; RWF Warfarin; SIE Solvated Interaction Energy; HUVEC human umbilical vein endothelial cells; H9c2 rat cardiomyoblasts.

REFERENCES

1. Go, A. S.; Mozaffarian, D.; Roger, V. L.; Benjamin, E. J.; Berry, J. D.; Blaha, M. J.; Dai, S.; Ford, E. S.; Fox, C. S.; Franco, S.; Fullerton, H. J.; Gillespie, C.; Hailpern, S. M.; Heit, J. A.; Howard, V. J.; Huffman, M. D.; Judd, S. E.; Kissela, B. M.; Kittner, S. J.; Lackland, D. T.; Lichtman, J. H.; Lisabeth, L. D.; Mackey, R. H.; Magid, D. J.; Marcus, G. M.; Marelli, A.; Matchar, D. B.; McGuire, D. K.; Mohler, E. R., 3rd; Moy, C. S.; Mussolino, M. E.; Neumar, R. W.; Nichol, G.; Pandey, D. K.; Paynter, N. P.; Reeves, M. J.; Sorlie, P. D.; Stein, J.; Towfighi, A.; Turan, T. N.; Virani, S. S.; Wong, N. D.; Woo, D.; Turner, M. B., Heart disease and stroke statistics--2014 update: a report from the American Heart Association. *Circulation* **2014,** *129* (3), e28-e292.
2. Nabel, E. G.; Braunwald, E., A Tale of Coronary Artery Disease and Myocardial Infarction. *New England Journal of Medicine* **2012,** *366* (1), 54-63.
3. de Boer, R. A.; van Veldhuisen, D. J., ACE-inhibitors, Beta-blockers or the Combination in Heart Failure: Is It Just an A–B–C? *Cardiovascular Drugs and Therapy* **2008,** *22* (4), 261-263.
4. Feneck, R., Phosphodiesterase inhibitors and the cardiovascular system. *Continuing Education in Anaesthesia, Critical Care & Pain* **2007,** *7* (6), 203-207.
5. Alousi, A.; Johnson, D., Pharmacology of the bipyridines: amrinone and milrinone. *Circulation* **1986,** *73* (3 Pt 2), III10-24.
6. Baim, D. S.; McDowell, A. V.; Cherniles, J.; Monrad, E. S.; Parker, J. A.; Edelson, J.; Braunwald, E.; Grossman, W., Evaluation of a new bipyridine inotropic agent—milrinone—in patients with severe congestive heart failure. *New England journal of medicine* **1983,** *309* (13), 748-756.
7. Young, R. A.; Ward, A., Milrinone. *Drugs* **1988,** *36* (2), 158-192.
8. Barton, P.; Garcia, J.; Kouatli, A.; Kitchen, L.; Zorka, A.; Lindsay, C.; Lawless, S.; Giroir, B., Hemodynamic effects of iv milrinone lactate in pediatric patients with septic shock: A prospective, double-blinded, randomized, placebo-controlled, interventional study. *CHEST Journal* **1996,** *109* (5), 1302-1312.
9. Wang, Z.; Wu, Q.; Nie, X.; Guo, J.; Yang, C., Combination therapy with milrinone and esmolol for heart protection in patients with severe sepsis: a prospective, randomized trial. *Clinical drug investigation* **2015,** *35* (11), 707-716.
10. Cuffe, M. S.; Califf, R. M.; Adams Jr, K. F.; Benza, R.; Bourge, R.; Colucci, W. S.; Massie, B. M.; O'Connor, C. M.; Pina, I.; Quigg, R., Short-term intravenous milrinone for acute exacerbation of chronic heart failure: a randomized controlled trial. *Jama* **2002,** *287* (12), 1541-1547.
11. Abbasi, S.; Paul, A.; Shao, W.; Prakash, S., Cationic albumin nanoparticles for enhanced drug delivery to treat breast cancer: preparation and in vitro assessment. *Journal of drug delivery* **2011,** *2012*.

12. Sebak, S.; Mirzaei, M.; Malhotra, M.; Kulamarva, A.; Prakash, S., Human serum albumin nanoparticles as an efficient noscapine drug delivery system for potential use in breast cancer: preparation and in vitro analysis. *International journal of nanomedicine* **2010,** *5*, 525.
13. Lomis, N.; Westfall, S.; Farahdel, L.; Malhotra, M.; Shum-Tim, D.; Prakash, S., Human Serum Albumin Nanoparticles for Use in Cancer Drug Delivery: Process Optimization and In Vitro Characterization. *Nanomaterials* **2016,** *6* (6), 116.
14. Edelson, J.; Stroshane, R.; Benziger, D. P.; Cody, R.; Benotti, J.; Hood Jr, W.; Chatterjee, K.; Luczkowec, C.; Krebs, C.; Schwartz, R., Pharmacokinetics of the bipyridines amrinone and milrinone. *Circulation* **1986,** *73* (3 Pt 2), III145-52.
15. Wang, F.; Yang, K.; Wang, Z.; Ma, Y.; Gutkind, J. S.; Hida, N.; Niu, G.; Tian, J., Combined image guided monitoring the pharmacokinetics of rapamycin loaded human serum albumin nanoparticles with a split luciferase reporter. *Nanoscale* **2016,** *8* (7), 3991-4000.
16. Al Kindi, H.; Paul, A.; You, Z.; Nepotchatykh, O.; Schwertani, A.; Prakash, S.; Shum-Tim, D., Sustained release of milrinone delivered via microparticles in a rodent model of myocardial infarction. *The Journal of thoracic and cardiovascular surgery* **2014,** *148* (5), 2316-2324.
17. Singh, R.; Lillard, J. W., Nanoparticle-based targeted drug delivery. *Experimental and molecular pathology* **2009,** *86* (3), 215-223.
18. Hawkins, M. J.; Soon-Shiong, P.; Desai, N., Protein nanoparticles as drug carriers in clinical medicine. *Advanced drug delivery reviews* **2008,** *60* (8), 876-885.
19. Grislain, L.; Couvreur, P.; Lenaerts, V.; Roland, M.; Deprez-Decampeneere, D.; Speiser, P., Pharmacokinetics and distribution of a biodegradable drug-carrier. *International Journal of Pharmaceutics* **1983,** *15* (3), 335-345.
20. Müller, R.; Maaben, S.; Weyhers, H.; Mehnert, W., Phagocytic uptake and cytotoxicity of solid lipid nanoparticles (SLN) sterically stabilized with poloxamine 908 and poloxamer 407. *Journal of drug targeting* **1996,** *4* (3), 161-170.
21. Elzoghby, A. O.; Samy, W. M.; Elgindy, N. A., Albumin-based nanoparticles as potential controlled release drug delivery systems. *Journal of controlled release* **2012,** *157* (2), 168-182.
22. Langer, K.; Balthasar, S.; Vogel, V.; Dinauer, N.; Von Briesen, H.; Schubert, D., Optimization of the preparation process for human serum albumin (HSA) nanoparticles. *International Journal of Pharmaceutics* **2003,** *257* (1), 169-180.
23. Weber, C.; Coester, C.; Kreuter, J.; Langer, K., Desolvation process and surface characterisation of protein nanoparticles. *International journal of pharmaceutics* **2000,** *194* (1), 91-102.
24. Siddiqui, M.; Tariq, A.; Ahmad, A.; Chaudhary, M.; Shrivastava, S.; Singh, R., Application of DDQ and p-chloranilic acid for the spectrophotometric estimation of milrinone in pharmaceutical formulations. *Asian Journal of Scientific Research* **2009,** *2* (3), 135-145.
25. Berman, H. M.; Westbrook, J.; Feng, Z.; Gilliland, G.; Bhat, T. N.; Weissig, H.; Shindyalov, I. N.; Bourne, P. E., The protein data bank. *Nucleic acids research* **2000,** *28* (1), 235-242.
26. Sulea, T.; Purisima, E. O., The solvated interaction energy method for scoring binding affinities. *Computational Drug Discovery and Design* **2012**, 295-303.
27. Hogues, H.; Sulea, T.; Purisima, E. O., Exhaustive docking and solvated interaction energy scoring: lessons learned from the SAMPL4 challenge. *Journal of computer-aided molecular design* **2014,** *28* (4), 417-427.

28. Clark, M.; Cramer, R. D.; Van Opdenbosch, N., Validation of the general purpose Tripos 5.2 force field. *Journal of Computational Chemistry* **1989,** *10* (8), 982-1012.
29. Sreerama, N.; Woody, R. W., On the analysis of membrane protein circular dichroism spectra. *Protein Science* **2004,** *13* (1), 100-112.
30. Böhm, G.; Muhr, R.; Jaenicke, R., Quantitative analysis of protein far UV circular dichroism spectra by neural networks. *Protein engineering* **1992,** *5* (3), 191-195.
31. Langer, K.; Anhorn, M.; Steinhauser, I.; Dreis, S.; Celebi, D.; Schrickel, N.; Faust, S.; Vogel, V., Human serum albumin (HSA) nanoparticles: reproducibility of preparation process and kinetics of enzymatic degradation. *International journal of pharmaceutics* **2008,** *347* (1), 109-117.
32. Fan, F.; Nie, S.; Yang, D.; Luo, M.; Shi, H.; Zhang, Y.-H., Labeling lysosomes and tracking lysosome-dependent apoptosis with a cell-permeable activity-based probe. *Bioconjugate chemistry* **2012,** *23* (6), 1309-1317.
33. Ghuman, J.; Zunszain, P. A.; Petitpas, I.; Bhattacharya, A. A.; Otagiri, M.; Curry, S., Structural basis of the drug-binding specificity of human serum albumin. *Journal of molecular biology* **2005,** *353* (1), 38-52.
34. Robertson, D. W.; Beedle, E.; Swartzendruber, J. K.; Jones, N. D.; Elzey, T.; Kauffman, R. F.; Wilson, H.; Hayes, J. S., Bipyridine cardiotonics: the three-dimensional structures of amrinone and milrinone. *Journal of medicinal chemistry* **1986,** *29* (5), 635-640.
35. Cody, V.; Wojtczak, A.; Davis, F. B.; Davis, P. J.; Blas, S. D., Structure-activity relationships of milrinone analogues determined in vitro in a rabbit heart membrane Ca (2+)-ATPase model. *Journal of medicinal chemistry* **1995,** *38* (11), 1990-1997.
36. Jun, J. Y.; Nguyen, H. H.; Chun, H. S.; Kang, B.-C.; Ko, S., Preparation of size-controlled bovine serum albumin (BSA) nanoparticles by a modified desolvation method. *Food Chemistry* **2011,** *127* (4), 1892-1898.
37. Damink, L. O.; Dijkstra, P.; Van Luyn, M.; Van Wachem, P.; Nieuwenhuis, P.; Feijen, J., Glutaraldehyde as a crosslinking agent for collagen-based biomaterials. *Journal of materials science: materials in medicine* **1995,** *6* (8), 460-472.
38. Kelly, S. M.; Jess, T. J.; Price, N. C., How to study proteins by circular dichroism. *Biochimica et Biophysica Acta (BBA)-Proteins and Proteomics* **2005,** *1751* (2), 119-139.
39. Ahmad, B.; Parveen, S.; Khan, R. H., Effect of albumin conformation on the binding of ciprofloxacin to human serum albumin: a novel approach directly assigning binding site. *Biomacromolecules* **2006,** *7* (4), 1350-1356.
40. Peters, T., Serum albumin. *Advances in protein chemistry* **1985,** *37*, 161-245.
41. Bian, Q.; Liu, J.; Tian, J.; Hu, Z., Binding of genistein to human serum albumin demonstrated using tryptophan fluorescence quenching. *International journal of biological macromolecules* **2004,** *34* (5), 275-279.
42. Neault, J.; Tajmir-Riahi, H., Interaction of cisplatin with human serum albumin. Drug binding mode and protein secondary structure. *Biochimica et Biophysica Acta (BBA)-Protein Structure and Molecular Enzymology* **1998,** *1384* (1), 153-159.
43. Chatterjee, T.; Pal, A.; Dey, S.; Chatterjee, B. K.; Chakrabarti, P., Interaction of virstatin with human serum albumin: spectroscopic analysis and molecular modeling. *PLoS One* **2012,** *7* (5), e37468.
44. Tiruppathi, C.; Song, W.; Bergenfeldt, M.; Sass, P.; Malik, A. B., Gp60 activation mediates albumin transcytosis in endothelial cells by tyrosine kinase-dependent pathway. *Journal of Biological Chemistry* **1997,** *272* (41), 25968-25975.

45. Popov, D.; Hasu, M.; Ghinea, N.; Simionescu, N.; Simionescu, M., Cardiomyocytes express albumin binding proteins. *Journal of molecular and cellular cardiology* **1992,** *24* (9), 989-1002.
46. Carter, D. C.; Ho, J. X., Structure of serum albumin. *Advances in protein chemistry* **1994,** *45*, 153-203.
47. Wilting, J.; van der Giesen, W. F.; Janssen, L.; Weideman, M.; Otagiri, M.; Perrin, J., The effect of albumin conformation on the binding of warfarin to human serum albumin. The dependence of the binding of warfarin to human serum albumin on the hydrogen, calcium, and chloride ion concentrations as studied by circular dichroism, fluorescence, and equilibrium dialysis. *Journal of Biological Chemistry* **1980,** *255* (7), 3032-3037.
48. Graciani, F. S.; Ximenes, V. F., Investigation of human albumin-induced circular dichroism in dansylglycine. *PloS one* **2013,** *8* (10), e76849.

For Table of Contents Only

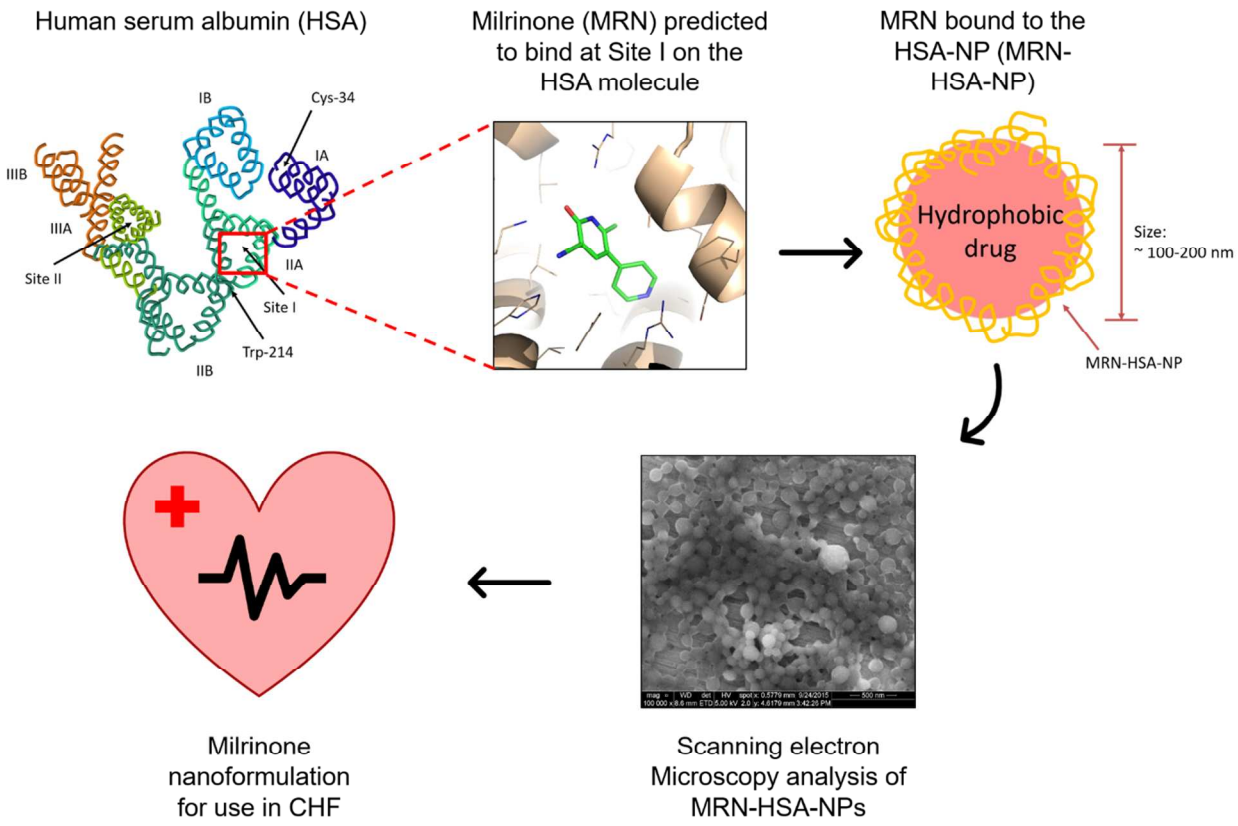

A novel milrinone nanoformulation for use in cardiovascular diseases: preparation and *in vitro* characterization

Figures and Tables

FIGURES

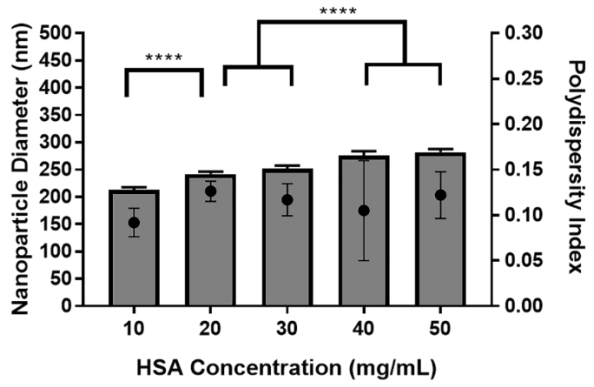

(a)

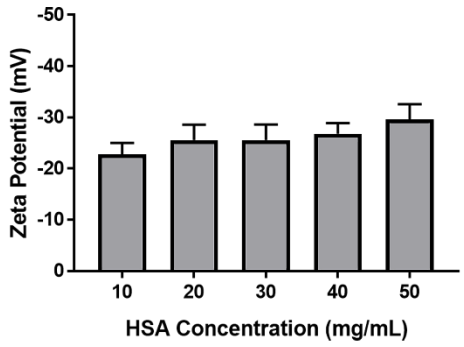

(b)

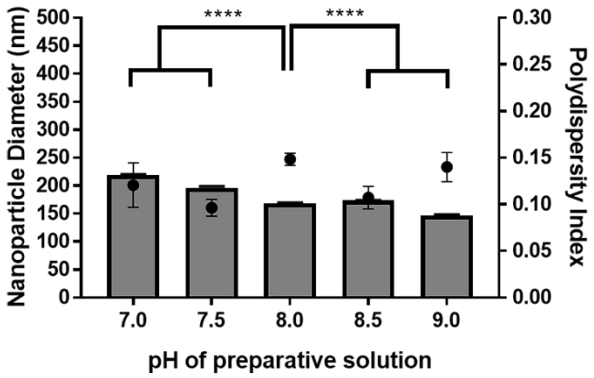

(c)

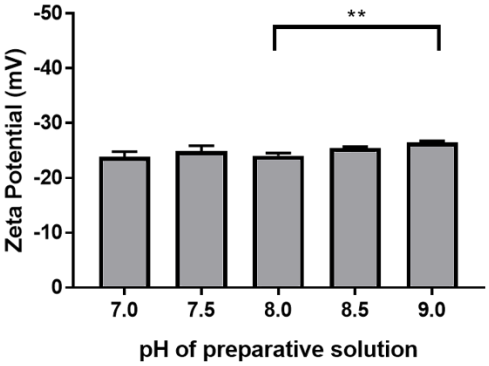

(d)

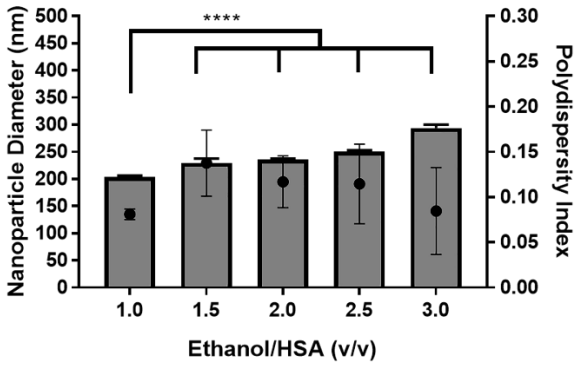

(e)

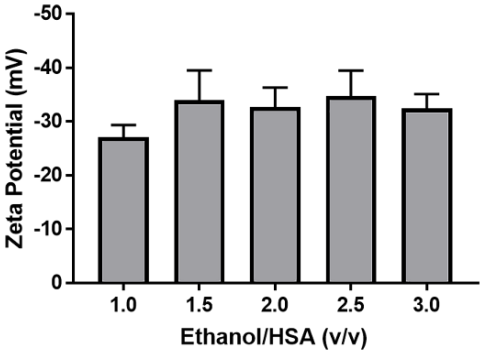

(f)

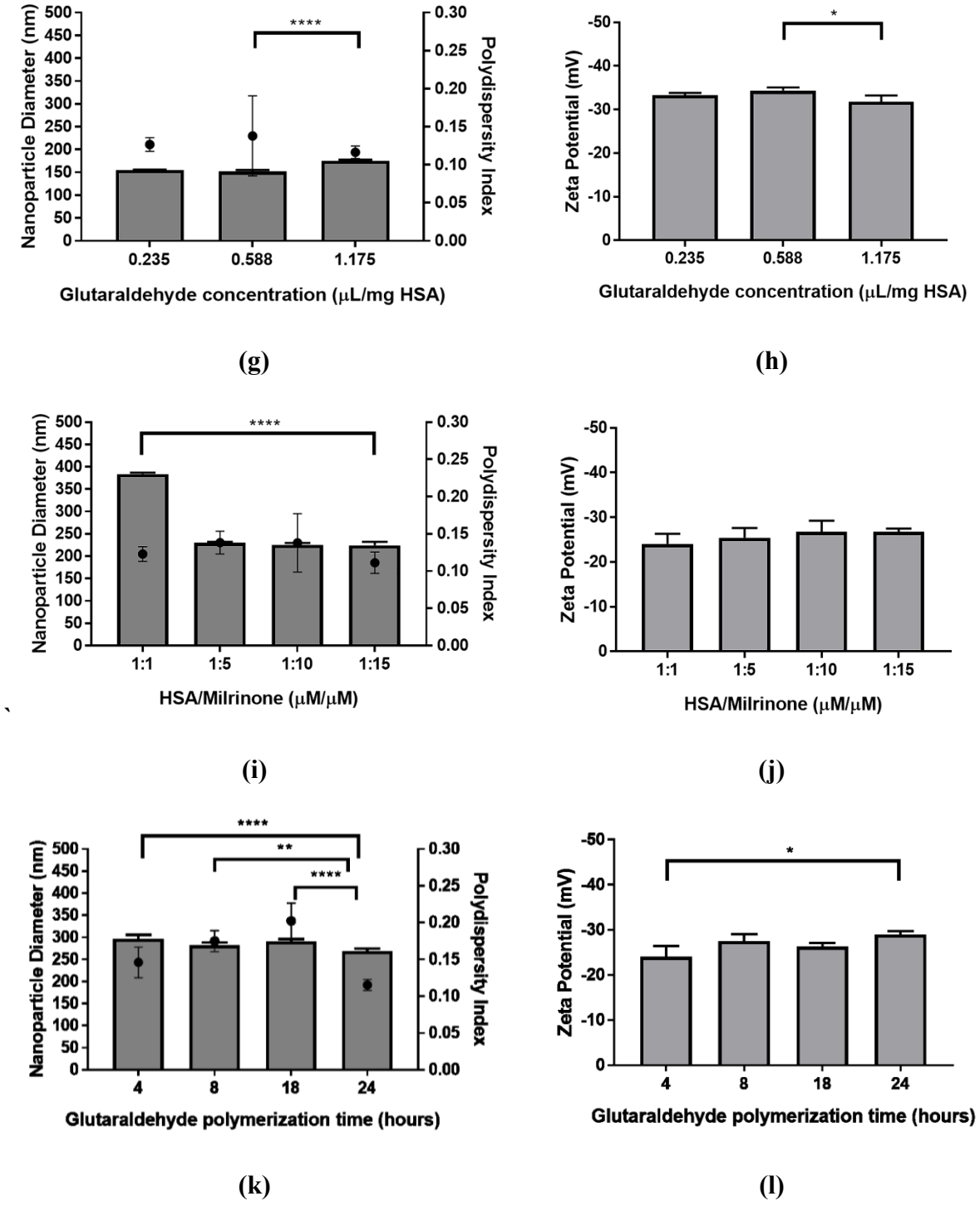

Figure 1. Effect of HSA concentration (mg/mL) on **(a)** nanoparticle diameter and polydispersity index and **(b)** nanoparticle zeta potential; Effect of pH of preparative solution on **(c)** nanoparticle diameter and polydispersity index and **(d)** nanoparticle zeta potential; Effect of ratio of ethanol/HSA (v/v) on **(e)** nanoparticle diameter and polydispersity index and **(f)** nanoparticle zeta potential; Effect of glutaraldehyde concentration (μL/mg HSA) on **(g)** nanoparticle diameter and polydispersity index and **(h)** nanoparticle zeta potential; Effect of HSA/Milrinone (μM/μM) ratio on **(i)** nanoparticle diameter and polydispersity index and **(j)** nanoparticle zeta potential; Effect of glutaraldehyde polymerization time (hours) on **(k)** nanoparticle

diameter and polydispersity index and **(l)** nanoparticle zeta potential. The nanoparticle diameter is represented as the dark grey bar, polydispersity index as symbol and zeta potential as light grey bar. The graphs show a representative result of mean±SD (n=3). ****P<0.0001 was considered highly significant and *** P<0.001, * P<0.05 were considered significant based on Tuckey's posthoc analysis, when compared with other groups.

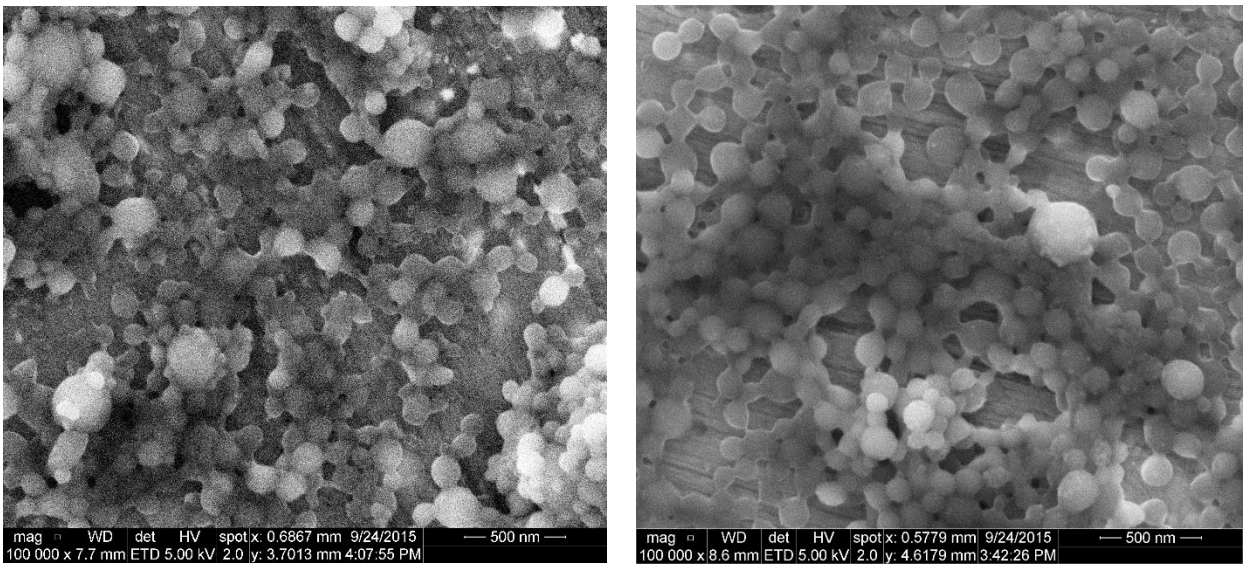

(**a**) (**b**)

Figure 2. Nanoparticle surface characterization using SEM analysis: **(a)** MRN-HSA-NPs of size 154.2±5.8 nm, polydispersity index of approximately 0.08 and zeta potential of -29.5±2.9 mV (Scale = 500 nm); **(b)** HSA-NPs of size 148.5±6.2 nm, polydispersity index of approximately 0.19 and zeta potential of -27.1±3.3 mV (Scale = 500 nm).

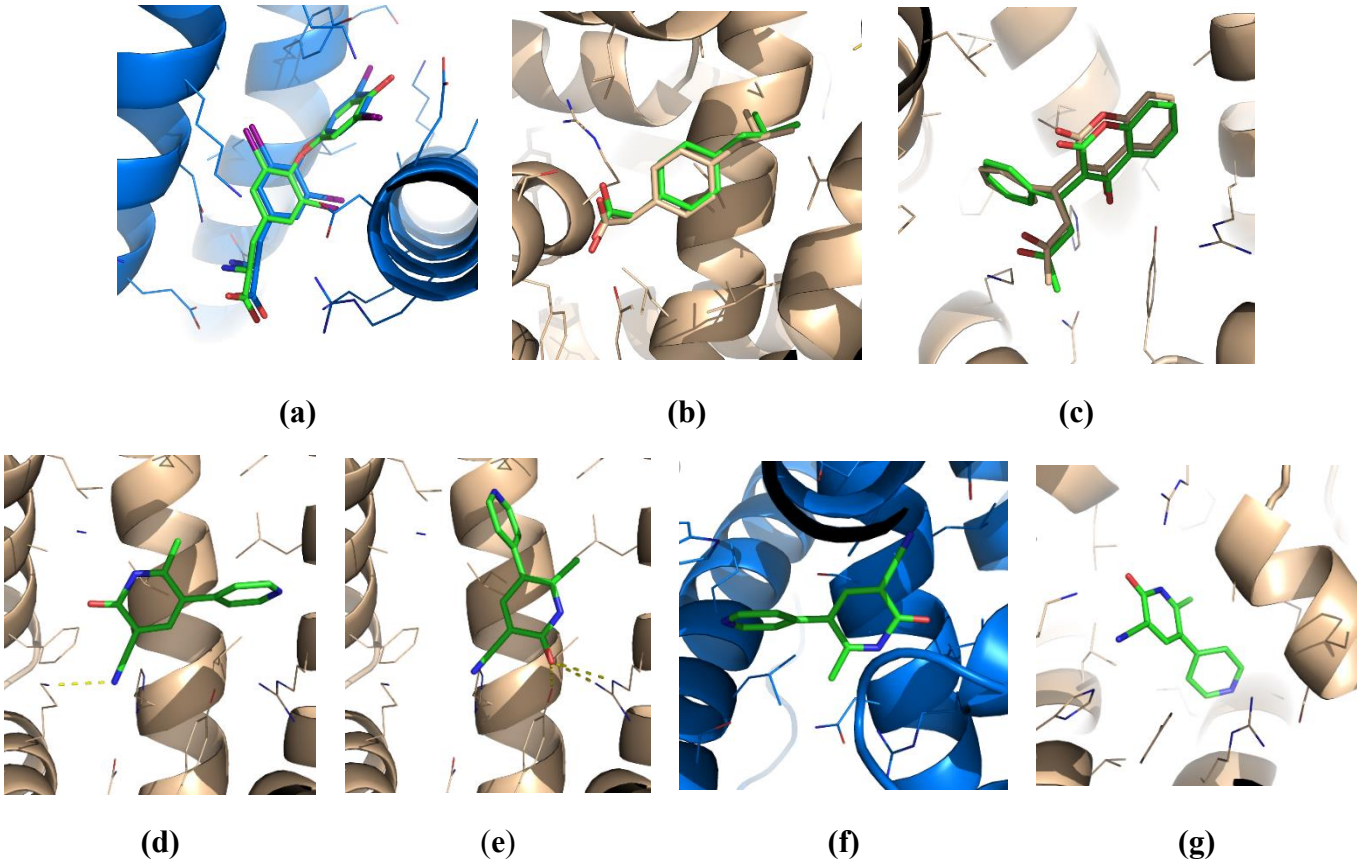

Figure 3. Molecular docking predictions for **(a)** Thyroxine (green) relative to its cognate conformation (blue); **(b)** Ibuprofen (green) relative to its cognate conformation (beige); **(c)** Warfarin (green) relative to its cognate conformation (beige); **(d)** MRN (green) docked against HSA, where the nitrile group on MRN forms 1 H-bond (yellow dashed line) with Lys195 on HSA; **(e)** MRN docked against HSA, where the hydroxyl group forms 3 H-bonds (yellow dashed lines) with Arg257 and Tyr150; **(f)** MRN (green) predicted to bind the strongest to forms of HSA bound to fatty acids, in the same sub-pocket as Warfarin when considering Wilma scoring results; **(g)** MRN (green) predicted to bind the strongest to forms of HSA unbound to fatty acids when considering SIE re-scoring results.

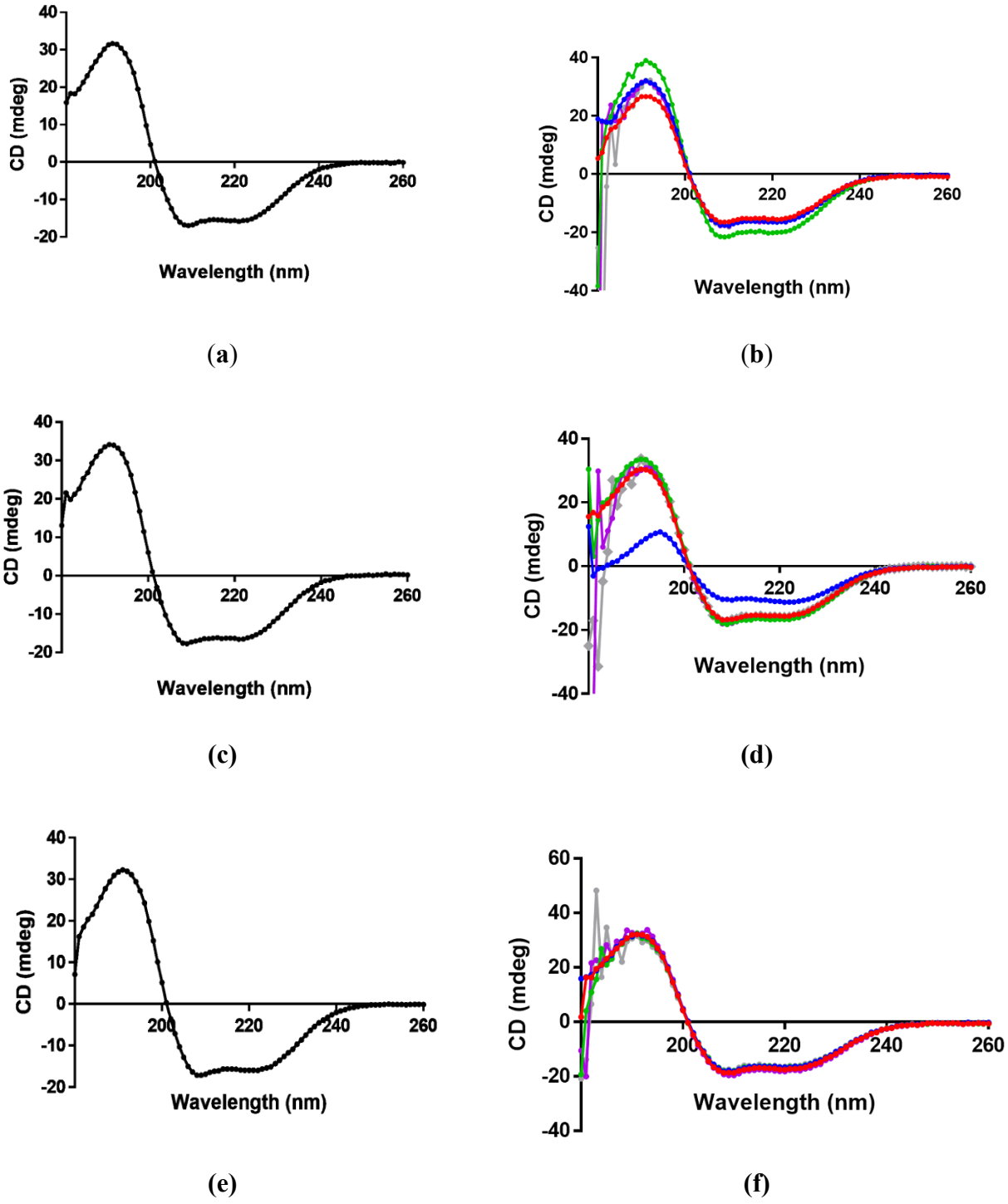

Figure 4. Far-UV CD spectra: **(a)** HSA at pH 7.0 **(b)** HSA at HSA/MRN molar ratios of 0 (dark blue), 1:1 (red), 1:5 (green), 1:10 (purple), 1:15 (light blue) and 1:20 (orange); **(c)** HSA at pH 8.0; **(d)** HSA at HSA/MRN molar ratios of 0 (dark blue), 1:1 (red), 1:5 (green), 1:10 (purple), 1:15 (light blue) and 1:20 (orange); **(e)** HSA at pH 9.0; **(f)** HSA at HSA/MRN molar ratios of 0 (dark blue), 1:1 (red), 1:5 (green), 1:10 (purple), 1:15 (light blue) and 1:20 (orange).

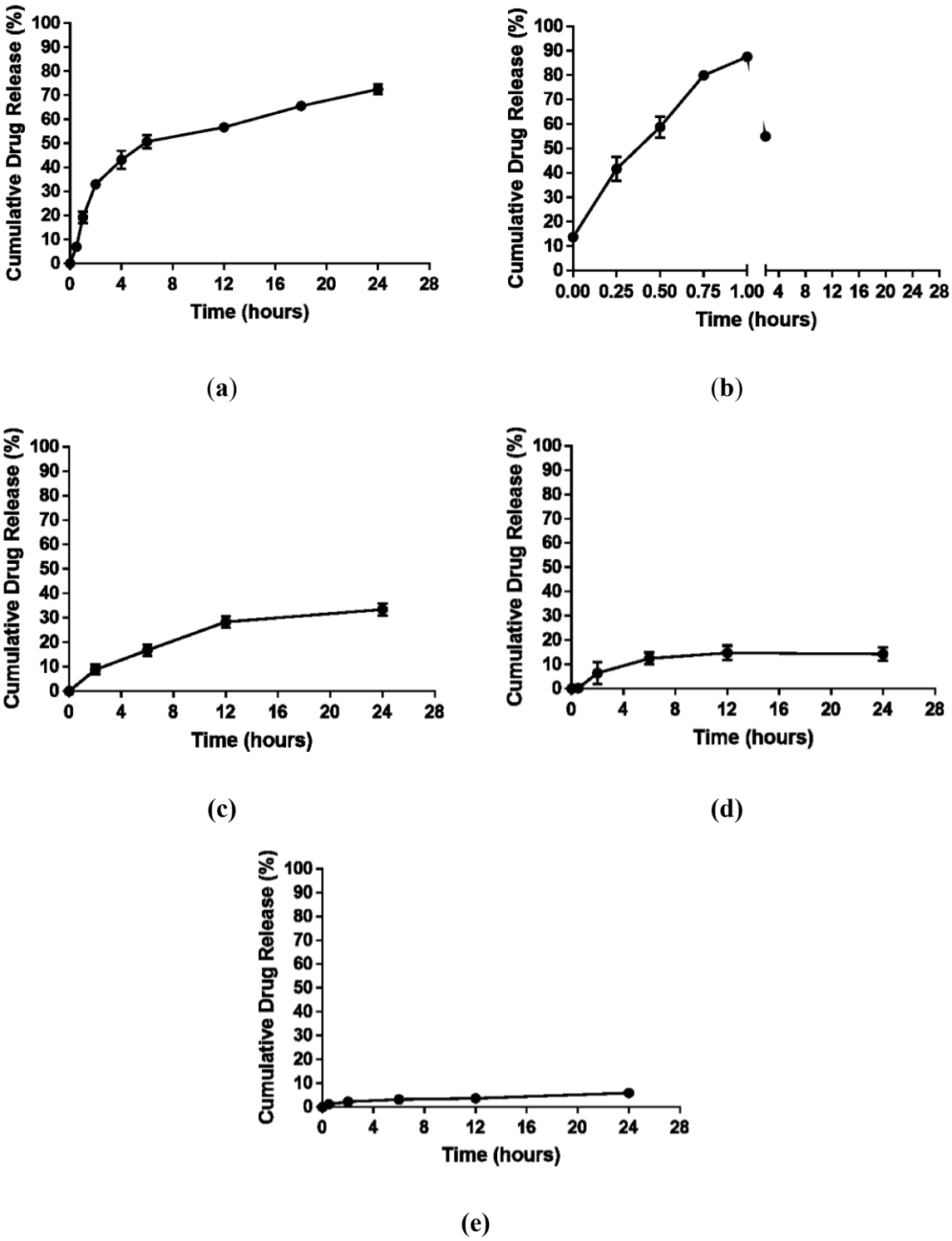

Figure 5. Cumulative release of MRN from 1 mg/mL MRN-HSA-NPs in the presence of **(a)** trypsin, **(b)** pepsin, **(c)** proteinase K, **(d)** protease and **(e)** cathepsin D. The graphs show a representative result of mean±SD (n=3).

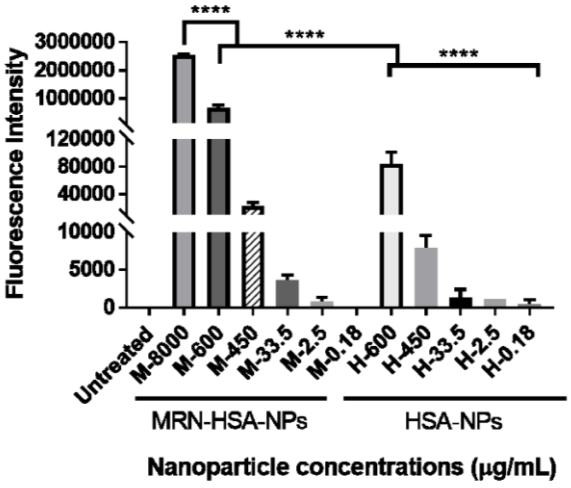

(a)

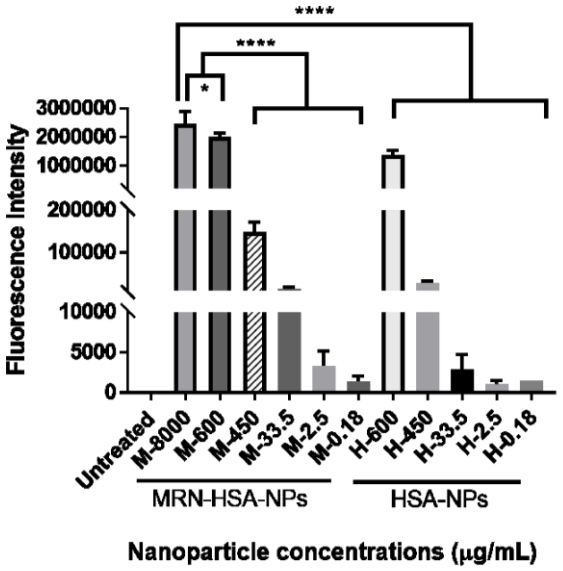

(b)

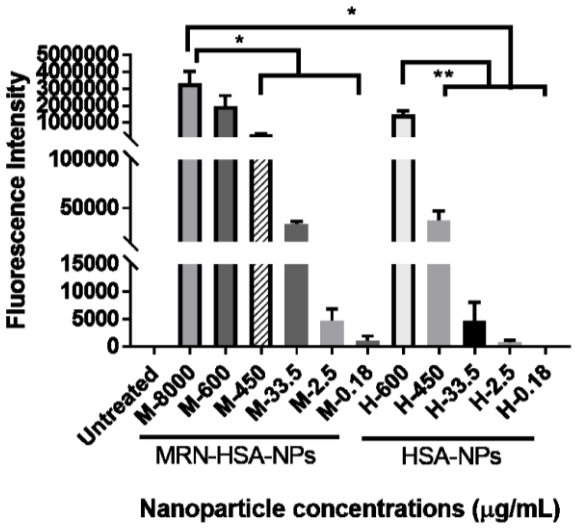

(c)

Figure 6. Intracellular uptake of MRN-HSA-NPs and HSA-NPs in HUVEC cells at **(a)** 4 hours, **(b)** 24 hours and **(c)** 48 hours. HUVEC cells were treated with different nanoparticle concentrations: 8000, 600, 450, 33.5, 2.5 and 0.18 μg/mL, represented as M-8000, M-600, M-450, M-33.5, M-2.5 and M-0.18 in case of MRN-HSA-NPs; and H-8000, H-600, H-450, H-33.5, H-2.5 and H-0.18 in case of HSA-NPs alone. The graph shows a representative result of mean±SD (n=3). ****P<0.0001 was considered highly significant and *** P<0.001, * P<0.05 were considered significant based on Tuckey's posthoc analysis, when compared with other groups.

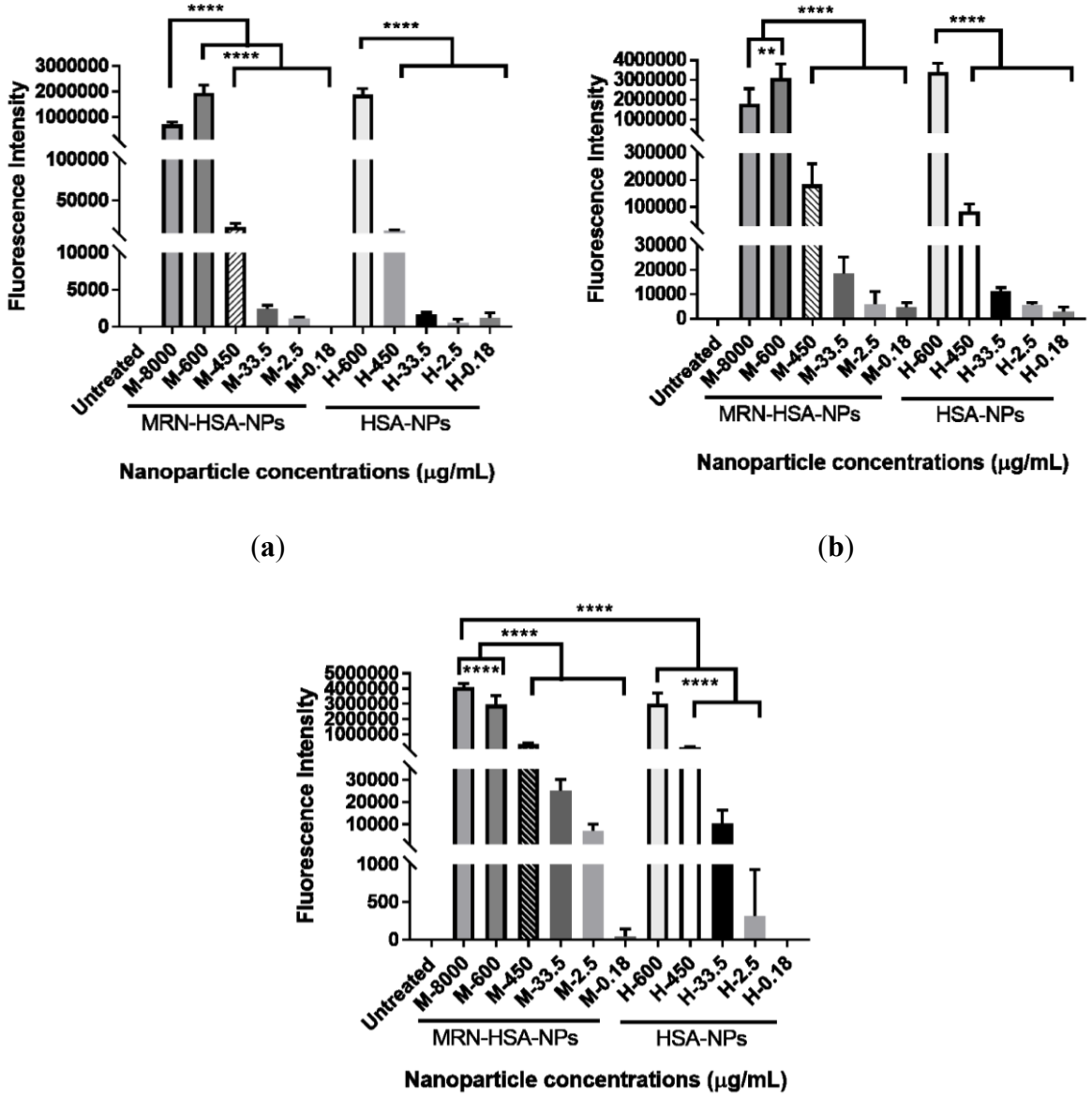

Figure 7. Intracellular uptake of MRN-HSA-NPs and HSA-NPs in H9c2 cells at **(a)** 4 hours, **(b)** 24 hours and **(c)** 48 hours. H9c2 cells were treated with different nanoparticle concentrations: 8000, 600, 450, 33.5, 2.5 and 0.18 μg/mL, represented as M-8000, M-600, M-450, M-33.5, M-2.5 and M-0.18 in case of MRN-HSA-NPs; and H-8000, H-600, H-450, H-33.5, H-2.5 and H-0.18 in case of HSA-NPs alone. The graph shows a representative result of mean±SD (n=3). ****P<0.0001 was considered highly significant and *** P<0.001, ** P<0.01 were considered significant based on Tuckey's posthoc analysis, when compared with other groups.

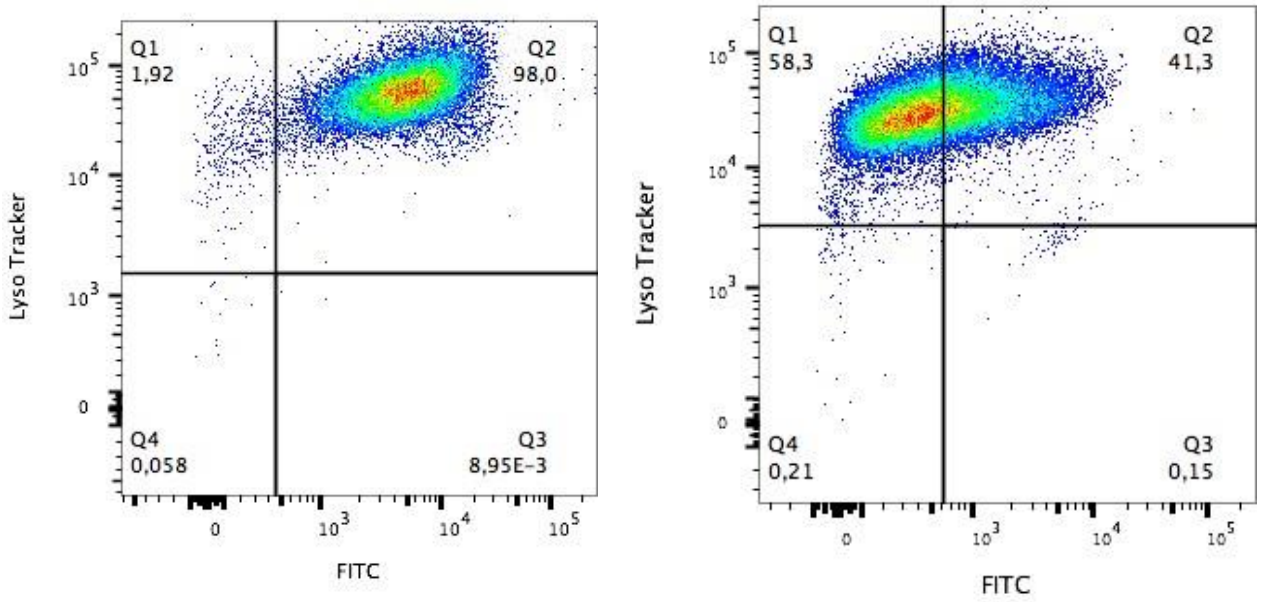

(**a**) **(b)**

Figure 8. Flow cytometry analysis of intracellular uptake of FITC-HSA-NPs. Gated on single cells and quadrants were set as per FMO controls. **(a)** HUVEC cells treated with both FITC-HSA-NPs and LysoTracker Deep Red exhibiting double staining in approximately 98% cell population (Q2 quadrant); **(b)** H9c2 cells treated with both FITC-HSA-NPs and LysoTracker Deep Red exhibiting double staining in approximately 41.3% cell population (Q2 quadrant) with approximately 58.3% cells displaying Lysotracker Deep Red staining (Q1 quadrant). Data is represented for n=3 experiments.

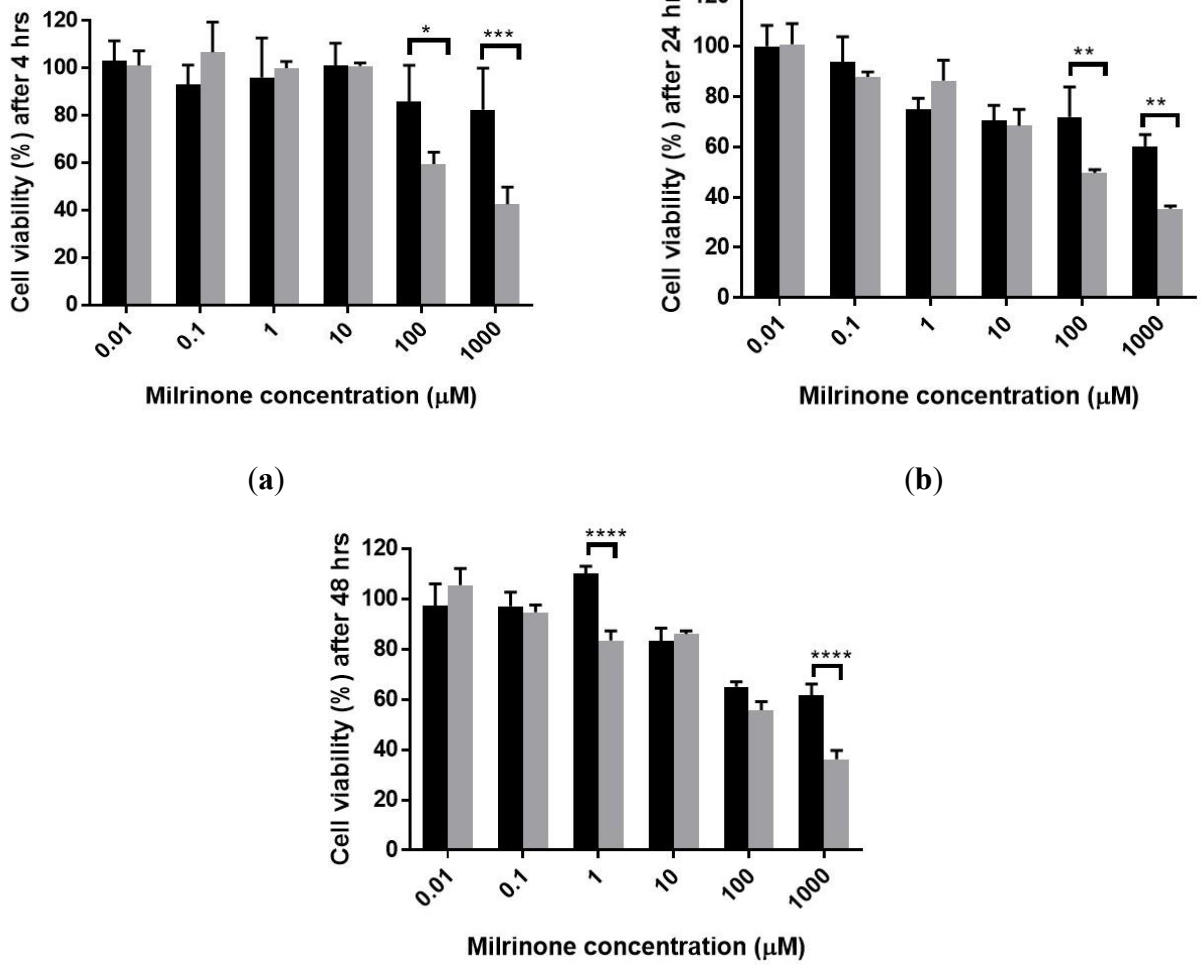

Figure 9. Viability of HUVECs incubated with MRN-HSA-NPs (black bars) compared with MRN-Lactate (grey bars) at different MRN concentrations, at **(a)** 4 hours, **(b)** 24 hours and **(c)** 48 hours. The graph shows a representative result of mean±SD (n=3). ****P<0.0001, ***P<0.001, **P<0.01 and *P<0.05 were considered significant based on Sidak's posthoc analysis.

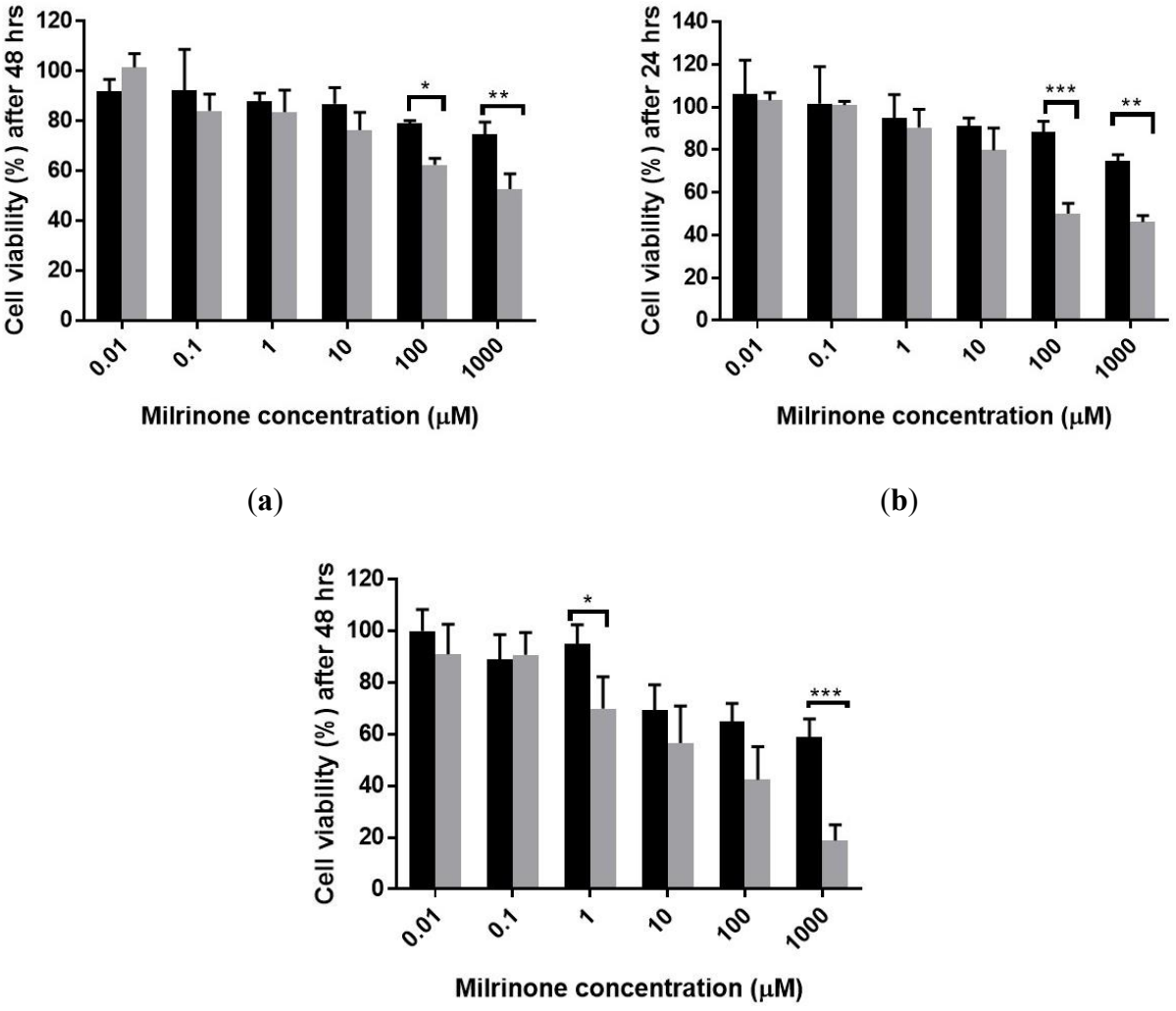

Figure 10. Viability of H9c2 cells incubated with MRN-HSA-NPs (black bars) compared with MRN-Lactate (grey bars) at different MRN concentrations, at **(a)** 4 hours, **(b)** 24 hours and **(c)** 48 hours. The graph shows a representative result of mean±SD (n=3). ****P<0.0001, ***P<0.001, **P<0.01 and *P<0.05 were considered significant based on Sidak's posthoc analysis.

TABLES

Table 1. Encapsulation efficiency of MRN-HSA-NPs at various MRN concentrations, represented as HSA/MRN molar ratio.

HSA/MRN molar ratio	Encapsulation efficiency (%)
1:1	86.9±13.8
1:5	23.4±4.9
1:10	30.2±5.9
1:15	41.8±1.7

Table 2. Predicted binding affinities between HSA and MRN using the Wilma and SIE scoring.

Ligand bound to HSA	SIE Predicted (kcal/mol)	Wilma Predicted (kcal/mol)
MRN (best Wilma)	-5.7	-27.6
MRN (best SIE)	-8.6	-26.5
THY (control)	-6.7	-26.2
RWF (control)	-8.3	-26.6
IBP (control)	-7.6	-23.6

Table 3: HSA secondary structural content on interaction with MRN in different molar ratios.

200 - 260 nm									
Molar ratio (HSA/MRN)	**HSA (at pH 7.0)**			**HSA (at pH 8.0)**			**HSA (at pH 9.0)**		
	α-helix (%)	**β-sheet (%)**	**Random coil (%)**	**α-helix (%)**	**β-sheet (%)**	**Random coil (%)**	**α-helix (%)**	**β-sheet (%)**	**Random coil (%)**
0	58.7	13.1	17.8	62.2	12.6	16.4	59.8	13.0	17.3
1:1	54.0	13.8	19.9	56.3	13.4	19.1	62.4	12.6	16.1
1:5	59.9	12.9	17.3	36.0	16.3	30.7	61.2	12.8	16.7
1:10	72.8	11.2	11.9	60.9	12.8	17.0	59.7	13.0	17.3
1:15	58.80	13.1	17.7	60.1	12.9	17.1	65.5	12.2	14.8
1:20	59.10	13.1	17.6	57.8	13.2	18.3	59.1	13.1	17.6

Table 4. Cumulative release of MRN from MRN-HSA-NPs in the presence of different enzymes.

Enzyme present with MRN-HSA-NPs	Cumulative MRN release (%)
Trypsin	72.5±1.9
Pepsin	87.5±0.9
Proteinase K	33.4±2.5
Protease	14.2±2.7
Cathepsin D	5.9±1.3